Domain Generalization using Causal Matching

Divyat Mahajan [1] **Shruti Tople** [2] **Amit Sharma** [1]

Abstract

In the domain generalization literature, a common objective is to learn representations independent of the domain after conditioning on the class label. We show that this objective is not sufficient: there exist counter-examples where a model fails to generalize to unseen domains even after satisfying class-conditional domain invariance. We formalize this observation through a structural causal model and show the importance of modeling *within-class* variations for generalization. Specifically, classes contain *objects* that characterize specific causal features, and domains can be interpreted as interventions on these objects that change non-causal features. We highlight an alternative condition: inputs across domains should have the same representation if they are derived from the same object. Based on this objective, we propose matching-based algorithms when base objects are observed (e.g., through data augmentation) and approximate the objective when objects are not observed (`MatchDG`). Our simple matching-based algorithms are competitive to prior work on out-of-domain accuracy for rotated MNIST, Fashion-MNIST, PACS, and Chest-Xray datasets. Our method `MatchDG` also recovers ground-truth *object matches*: on MNIST and Fashion-MNIST, top-10 matches from `MatchDG` have over 50% overlap with ground-truth matches.

1. Introduction

Domain generalization is the task of learning a machine learning model that can generalize to unseen data distributions, after training on more than one data distributions. For example, a model trained on hospitals in one region may be deployed to another, or an image classifier may be deployed on slightly rotated images. Typically, it is assumed that the different domains share some "stable" features whose relationship with the output is invariant across domains (Piratla et al., 2020) and the goal is to learn those features. A popular class of methods aim to learn representations that are independent of domain *conditional on class* (Li et al., 2018c;d; Ghifary et al., 2016; Hu et al., 2019), based on evidence of their superiority (Zhao et al., 2019) to methods that learn representations that are marginally independent of domain (Muandet et al., 2013; Ganin et al., 2016).

In this work, we show that the class-conditional domain-invariant objective for representations is insufficient. We provide counter-examples where a feature representation satisfies the objective but still fails to generalize to new domains, both theoretically and empirically. Specifically, when the distribution of the stable features to be learnt varies across domains, class-conditional objective is insufficient to learn the stable features (they are optimal only when the distribution of stable features is the same across domains). Differing distributions of stable features within the same class label is common in real-world datasets, e.g., in digit recognition, the stable feature *shape* may differ based on people's handwriting, or medical images may differ based on variation in body characteristics across people. Our investigation reveals the importance of considering within-class variation in the stable features.

To derive a better objective for domain generalization, we represent the within-class variation in stable features using a structural causal model, building on prior work (Heinze-Deml & Meinshausen, 2019) from single-domain generalization. Specifically, we construct a model for the data generation process that assumes each input is constructed from a mix of stable (*causal*) and domain-dependent (*non-causal*) features, and only the stable features cause the output. We consider domain as a special intervention that changes the non-causal features of an input, and posit that an ideal classifier should be based only on the causal features. Using d-separation, we show that the correct objective is to build a representation that is invariant conditional on each *object*, where an object is defined as a set of inputs that share the same causal features (e.g., photos of the same person from different viewpoints or augmentations of an image in different rotations, color or background). When the object variable is observed (e.g., in self-collected data or by dataset augmentation), we propose a *perfect-match* regularizer for

[1]Microsoft Research, India [2]Microsoft Research, UK.. Correspondence to: Divyat Mahajan <divyatmahajan@gmail.com>.

Proceedings of the 38^{th} International Conference on Machine Learning, PMLR 139, 2021.

domain generalization that minimizes the distance between representations of the same object across domains.

In practice, however, the underlying objects are not always known. We therefore propose an approximation that aims to learn which inputs share the same object, under the assumption that inputs from the same class have more similar causal features than those from different classes. Our algorithm, `MatchDG` is an iterative algorithm that starts with randomly matched inputs from the same class and builds a representation using contrastive learning such that inputs sharing the same causal features are closer to one another. While past work has used contrastive loss to regularize the empirical risk minimization (ERM) objective (Dou et al., 2019), we demonstrate the importance of a two-phase method that first learns a representation independent of the ERM loss, so that classification loss does not interfere with the learning of stable features. In datasets with data augmentations, we extend `MatchDG` to also use the perfect object matches obtained from pairs of original and augmented images (`MDGHybrid`).

We evaluate our matching-based methods on rotated MNIST and Fashion-MNIST, PACS and Chest X-ray datasets. On all datasets, the simple methods `MatchDG` and `MDGHybrid` are competitive to state-of-the-art methods for out-of-domain accuracy. On the rotated MNIST and Fashion-MNIST datasets where the ground-truth objects are known, `MatchDG` learns to makes the representation more similar to their ground-truth matches (about 50% overlap for top-10 matches), even though the method does not have access to them. Our results with simple matching methods show the importance of enforcing the correct invariance condition.

Contributions. To summarize, our contributions include: **1).** An object-invariant condition for domain generalization that highlights a key limitation of previous approaches, **2).** When object information is not available, a two-phase, iterative algorithm to approximate object-based matches. Also, the code repository can be accessed at: `https://github.com/microsoft/robustdg`

2. Related Work

Learning common representation. To learn a generalizable classifier, several methods enforce the learnt representation $\Phi(\mathbf{x})$ to be independent of domain marginally or conditional on class label, using divergence measures such as maximum mean discrepancy (Muandet et al., 2013; Li et al., 2018b;c), adversarial training with a domain discriminator (Ganin et al., 2016; Li et al., 2018d; Albuquerque et al., 2020a), discriminant analysis (Ghifary et al., 2016; Hu et al., 2019), and other techniques (Ghifary et al., 2015).

Among them, several works (Zhao et al., 2019; Johansson et al., 2019; Akuzawa et al., 2019) show that the class-conditional methods (Li et al., 2018c;d; Ghifary et al., 2016; Hu et al., 2019) are better than those that enforce marginal domain-invariance of features (Muandet et al., 2013; Ganin et al., 2016; Li et al., 2018b; Albuquerque et al., 2020a), whenever there is a varying distribution of class labels across domains. We show that the class-conditional invariant is also not sufficient for generalizing to unseen domains.

Causality and domain generalization. Past work has shown the connection between causality and generalizable predictors (Peters et al., 2016; Christiansen et al., 2020). There is work on use of causal reasoning for domain adaptation (Gong et al., 2016; Heinze-Deml & Meinshausen, 2019; Magliacane et al., 2018; Rojas-Carulla et al., 2018) that assumes $Y \rightarrow X$ direction and other work (Arjovsky et al., 2019; Peters et al., 2016) on connecting causality that assumes $X \rightarrow Y$. Our SCM model unites these streams by introducing Y_{true} and labelled Y and develop an invariance condition for domain generalization that is valid under both interpretations. Perhaps the closest to our work is by (Heinze-Deml & Meinshausen, 2019) who use the object concept in single-domain datasets for better generalization. We extend their SCM to the multi-domain setting and use it to show the inconsistency of prior methods. In addition, while (Heinze-Deml & Meinshausen, 2019) assume objects are always observed, we also provide an algorithm for the case when objects are unobserved.

Matching and Contrastive Loss. Regularizers based on matching have been proposed for domain generalization. (Motiian et al., 2017) proposed matching representations of inputs from the same class. (Dou et al., 2019) used a contrastive (triplet) loss to regularize the ERM objective. In contrast to regularizing based on contrastive loss, our algorithm `MatchDG` proceeds in two phases and learns a representation independent of the ERM objective. Such an iterative 2-phase algorithm has empirical benefits, as we will show in Suppl. D.4. Additionally, we propose an ideal object-based matching algorithm when objects are observed.

Other work. Others approaches to domain generalization include meta-learning (Li et al., 2018a; Balaji et al., 2018), dataset augmentation (Volpi et al., 2018; Shankar et al., 2018), parameter decomposition (Piratla et al., 2020; Li et al., 2017), and enforcing domain-invariance of the optimal $P(Y|\Phi(\mathbf{x}))$ (Arjovsky et al., 2019; Ahuja et al., 2020). We empirically compare our algorithm to some of them.

3. Insufficiency of class-conditional invariance

Consider a classification task where the learning algorithm has access to i.i.d. data from m domains, $\{(d_i, \mathbf{x}_i, y_i)\}_{i=1}^n \sim (D_m, \mathcal{X}, \mathcal{Y})^n$ where $d_i \in D_m$ and $D_m \subset \mathcal{D}$ is a set of m domains. Each training input $(d, \mathbf{x}, y)$ is sampled from an unknown distribution

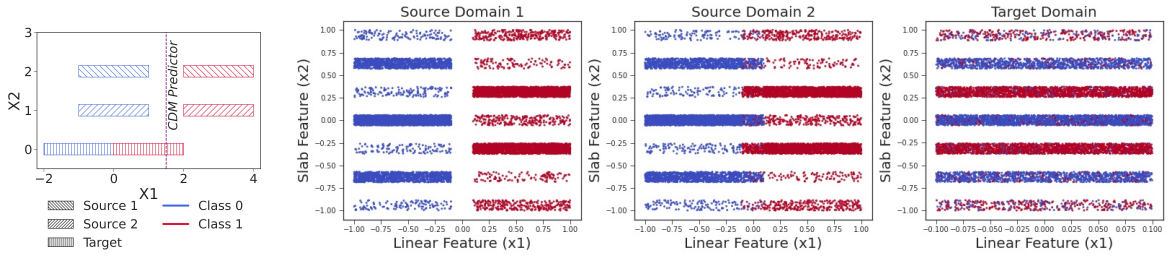

(a) Simple Example (b) Slab Dataset (*Slab (y-axis) is the stable feature)*

Figure 1. Two datasets showing the limitations of class-conditional domain-invariance objective. a) The CDM predictor is domain-invariant given the class label but does not generalize to the target domain; b) Colors denote the two ground-truth class labels. For class prediction, the linear feature exhibits varying level of noise across domains. The stable slab feature also has noise but it is invariant across domains.

$\mathcal{P}_m(D, X, Y)$. The domain generalization task is to learn a single classifier that generalizes well to unseen domains $d' \notin D_m$ and to new data from the same domains (Shankar et al., 2018). The optimum classifier can be written as: $f^* = \arg\min_{f \in \mathcal{F}} \mathbb{E}_{(d,\mathbf{x},y)\sim\mathcal{P}}[l(y^{(d)}, f(\mathbf{x}^{(d)}))]$, where $(d, \mathbf{x}, y) \sim \mathcal{P}$ over $(\mathcal{D}, \mathcal{X}, \mathcal{Y})$.

As mentioned above, a popular line of work enforces that the learnt representation $\Phi(\mathbf{x})$ be independent of domain conditional on the class (Li et al., 2018c;d; Ghifary et al., 2016; Hu et al., 2019), $\Phi(\mathbf{x}) \perp\!\!\!\perp D|Y$. Below we present two counter-examples showing that the class-conditional objective is not sufficient.

3.1. A simple counter-example

We construct an example where $\Phi(\mathbf{x}) \perp\!\!\!\perp D|Y$, but still the classifier does not generalize to new domains. Consider a two dimensional problem where $x_1 = x_c + \alpha_d; x_2 = \alpha_d$ where x_c and α_d are unobserved variables, and α_d varies with domain (Figure 1(a)). The true function depends only on the stable feature x_c, $y = f(x_c) = I(x_c \geq 0)$. Suppose there are two training domains with $\alpha_1 = 1$ for domain 1 and $\alpha_2 = 2$ for domain 2, and the test domain has $\alpha_3 = 0$ (see Figure 1(a)). Suppose further that the conditional distribution of X_C given Y is a uniform distribution that changes across domains: for domain 1, $X_c|Y = 1 \sim \mathcal{U}(1, 3); X_c|Y = 0 \sim \mathcal{U}(-2, 0)$; and for domain 2, $X_c|Y = 1 \sim \mathcal{U}(0, 2); X_c|Y = 0 \sim \mathcal{U}(-3, -1)$. Note that the distributions are picked such that $\phi(x_1, x_2) = x_1$ satisfies the conditional distribution invariant, $\phi(x) \perp\!\!\!\perp D|Y$. The optimal ERM classifier based on this representation, ($I(x_1 \geq 1.5)$ has 100% train accuracy on both domains. But for the test domain with $\alpha_d = 0; X_c|Y = 1 \sim \mathcal{U}(0, 2); X_c|Y = 0 \sim U(-2, 0)$, the classifier fails to generalize. It obtains 62.5% test accuracy (and 25% accuracy on the positive class), even though its representation satisfies class-conditional domain invariance. In comparison, the ideal representation is $x_1 - x_2$ which attains 100% train accuracy and 100% test domain accuracy, and does not satisfy the class-conditional invariant.

The above counter-example is due to the changing distribution of x_c across domains. If $P(X_c|Y)$ stays the same across domains, then class-conditional methods would not incorrectly pick x_1 as the representation. Following (Akuzawa et al., 2019), we claim the following (proof in Suppl. B.3).

Proposition 1. *Under the domain generalization setup as above, if $P(X_c|Y)$ remains the same across domains where x_c is the stable feature, then the class-conditional domain-invariant objective for learning representations yields a generalizable classifier such that the learnt representation $\Phi(\mathbf{x})$ is independent of the domain given x_c. Specifically, the entropy $H(d|x_c) = H(d|\Phi, x_c)$.*

However, if $P(X_C|Y)$ changes across domains, then we cannot guarantee the same: $H(d|x_c)$ and $H(d|\Phi, x_c)$ may not be equal. For building generalizable classifiers in such cases, this example shows that we need an additional constraint on Φ, $H(d|x_c) = H(d|\Phi, x_c)$; i.e. domain and representation should be independent conditioned on x_c.

3.2. An empirical study of class-conditional methods

As a more realistic example, consider the slab dataset introduced for detecting simplicity bias in neural networks (Shah et al., 2020) that contains a feature with spurious correlation. It comprises of two features and a binary label; (x_1) has a linear relationship with the label and the other feature (x_2) has a piece-wise linear relationship with the label which is a stable relationship. The relationship of the linear feature with the label changes with domains (A.1); we do so by adding noise with probability $\epsilon = 0$ for domain 1 and $\epsilon = 0.1$ for domain 2. On the third (test) domain, we add noise with probability 1 (see Figure 1(b)). We expect that methods that rely on the spurious feature x_1 would not be able to perform well on the out-of-domain data.

The results in Table 1 (implementation details in Appendix A.1) show that ERM is unable to learn the slab feature, as evident by poor generalization to the target domain, de-

spite very good performance on the source domains. We also show that methods based on learning invariant representations by unconditional (DANN, MMD, CORAL) and conditional distribution matching (CDANN, C-MMD, C-CORAL), and matching same-class inputs (RandomMatch) (Motiian et al., 2017) fail to learn the stable slab feature. Note that Proposition 1 suggested the failure of conditional distribution matching (CDM) algorithms when the distribution of stable feature (slab feature) is different across the source domains. However, the slab dataset has similar distribution of stable feature (slabs) across the source domains, yet the CDM algorithms fail to generalize to the target domain. It can be explained by considering the spurious linear feature, which can also satisfy the CDM constraint by "shifting" the y-conditional distributions along the linear feature. We conjecture that the model may first learn the linear feature due to its simplicity (Shah et al., 2020), and then retain the spurious linear feature upon further optimization since it satisfies the CDM constraint. This shows that the CDM methods can empirically fail even when there is an equal distribution of stable features across domains.

How can we ensure that a model learns the stable, generalizable feature x_2? We turn to our example above, where the required invariant was that the representation $\Phi(\mathbf{x})$ should be independent of domain given the stable feature. We apply this intuition and construct a model that enforces that the learnt representation be independent of domain given x_2. We do so by minimizing the ℓ_2-norm of the representations for data points from different domains that share the same slab value (details of the *PerfectMatch* method in Section 4.3). The results improve substantially: out-of-domain accuracy is now 78%.

In the next section, we formalize the intuition of conditioning on stable features x_c using a causal graph, and introduce the concept of *objects* that act as proxies of stable features.

Table 1. Slab Dataset: Source domains with noisy linear component with probability 0.0 and 0.1, target domain with noise 1.0. Mean and standard deviation over 10 different seed values for each method. The results for DANN (Ganin et al., 2016), CDANN (Li et al., 2018d), MMD, C-MMD (Li et al., 2018b), CORAL, C-CORAL (Sun & Saenko, 2016) were computed by using their implementations in DomainBed (Gulrajani & Lopez-Paz, 2020).

Method	Source 1	Source 2	Target
ERM	**100.0** (0.0)	96.0 (0.25)	57.6 (6.58)
DANN	99.9 (0.07)	94.8 (0.25)	53.0 (1.41)
MMD	99.9 (0.01)	95.9 (0.27)	62.9 (5.01)
CORAL	99.9 (0.01)	96.0 (0.27)	63.1 (5.86)
RandMatch	**100.0** (0.0)	96.1 (0.22)	59.5 (3.50)
CDANN	99.9 (0.01)	96.0 (0.27)	55.9 (2.47)
C-MMD	99.9 (0.01)	96.0 (0.27)	58.9 (3.43)
C-CORAL	99.9 (0.01)	96.0 (0.27)	64.7 (4.69)
PerfMatch	99.9 (0.05)	**97.8** (0.28)	**77.8** (6.01)

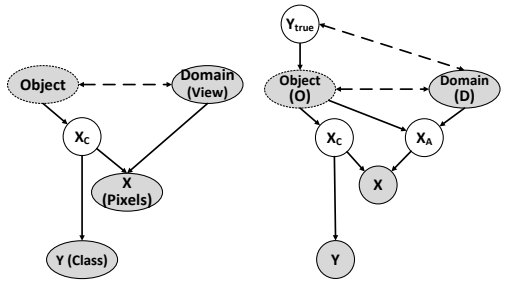

(a) Image classification. (b) General SCM.

Figure 2. Structural causal models for the data-generating process. Observed variables are shaded; dashed arrows denote correlated nodes. *Object* may not be observed.

4. A Causal View of Domain Generalization

4.1. Data-generating process

Figure 2(a) shows a structural causal model (SCM) that describes the data-generating process for the domain generalization task. For intuition, consider a task of classifying the type of item or screening an image for a medical condition. Due to human variability or by design (using data augmentation), the data generation process yields variety of images for each class, sometimes multiple views for the *same object*. Here each view can be considered as a different *domain* D, the label for item type or medical condition as the class Y, and the image pixels as the features X. Photos of the same item or the same person correspond to a common *object* variable, denoted by O. To create an image, the data-generating process first samples an object and view (domain) that may be correlated to each other (shown with dashed arrows). The pixels in the photo are caused by both the object and the view, as shown by the two incoming arrows to X. The object also corresponds to high-level *causal* features X_C that are common to any image of the same object, which in turn are used by humans to label the class Y. We call X_C as causal features because they directly cause the class Y.

The above example is typical of a domain generalization problem; a general SCM is shown in Figure 2(b), similar to the graph in (Heinze-Deml & Meinshausen, 2019). In general, the underlying *object* for each input $\mathbf{x}_i^{(d)}$ may not be observed. Analogous to the object-dependent (*causal*) features X_C, we introduce a node for domain-dependent high-level features of the object X_A. Changing the domain can be seen as an intervention: for each observed $\mathbf{x}_i^{(d)}$, there are a set of (possibly unobserved) counterfactual inputs $\mathbf{x}_j^{(d')}$ where $d \neq d'$, such that all correspond to the same object (and thus share the same X_C). For completeness, we also show the true unobserved label of the object which led to its generation as Y_{true} (additional motivation for the

causal graph is in Suppl. B.1). Like the object O, Y may be correlated with the domain D. Extending the model in (Heinze-Deml & Meinshausen, 2019), we allow that objects can be correlated with the domain conditioned on Y_{true}. As we shall see, considering the relationship of the *object* node becomes the key piece for developing the invariant condition. The SCM corresponds to the following non-parametric equations.

$$o := g_o(y_{true}, \epsilon_o, \epsilon_{od}) \qquad \mathbf{x}_c = g_{xc}(o)$$
$$\mathbf{x}_a := g_{xa}(d, o, \epsilon_{xa}) \qquad \mathbf{x} := g_x(\mathbf{x}_c, \mathbf{x}_a, \epsilon_x) y := h(\mathbf{x}_c, \epsilon_y)$$

where g_o, g_{xc}, g_{xa}, g_x and h are general non-parametric functions. The error ϵ_{od} is correlated with domain d whereas ϵ_o, ϵ_{xa}, ϵ_x and ϵ_y are mutually independent error terms that are independent of all other variables. Thus, noise in the class label is independent of domain. Since x_c is common to all inputs of the same object, g_{xc} is a deterministic function of o. In addition, the SCM provides conditional-independence conditions that all data distributions $\mathcal{P}$ must satisfy, through the concept of d-separation (Suppl. B.2) and the perfect map assumption (Pearl, 2009).

4.2. Identifying the invariance condition

From Figure 2(b), X_C is the node that causes Y. Further, by d-separation, the class label is independent of domain conditioned on X_C, $Y \perp\!\!\!\perp D | X_C$. Thus our goal is to learn y as $h(\mathbf{x}_c)$ where $h : \mathcal{C} \to \mathcal{Y}$. The ideal loss-minimizing function f^* can be rewritten as (assuming $\mathbf{x}_c$ is known):

$$\arg\min_f \mathbb{E}_{(d,\mathbf{x},y)} l(y, f(\mathbf{x})) = \arg\min_h \mathbb{E}[l(y, h(\mathbf{x}_c))] \qquad (1)$$

Since X_C is unobserved, this implies that we need to learn it through a representation function $\Phi : \mathcal{X} \to \mathcal{C}$. Together, $h(\Phi(x))$ leads to the desired classifer $f : \mathcal{X} \to \mathcal{Y}$.

Negative result on identification. Identification of causal features is a non-trivial problem (Magliacane et al., 2018). We first show that x_C is unidentifiable given observed data $P(X, Y, D, O)$ over multiple domains. Given the same probability distribution $P(X, Y, D, O)$, multiple values of X_C are possible. Substituting for o in the SCM equations, we obtain, $y = h(g_{xc}(o), \epsilon_y); \mathbf{x} = g_x(g_{xc}(o), g_{xa}(d, o, \epsilon_{xa}), \epsilon_x)$. By choosing g_x and h appropriately, different values of g_{xc} (that determine x_c from o) can lead to the same observed values for (y, d, o, x). The proof for the following proposition is in Supp. B.4.

Proposition 2. *Given observed data distribution $P(Y, X, D, O)$ that may also include data obtained from interventions on domain D, multiple values of X_C yield exactly the same observational and interventional distributions and hence X_c is unidentifiable.*

4.3. A "perfect-match" invariant

In the absence of identifiability, we proceed to find an invariant that can characterize X_c. By the d-separation criterion, we see that X_C satisfies two conditions: **1)** $X_C \perp\!\!\!\perp D | O$, **2)** $X_C \not\perp\!\!\!\perp O$; where O refers to the object variable and D refers to a domain. The first is an invariance condition: X_C does not change with different domains for the same object. To enforce this, we stipulate that the average pairwise distance between $\Phi(x)$ for inputs across domains for the same object is 0, $\sum_{\Omega(j,k)=1; d \neq d'} \text{dist}(\Phi(\mathbf{x}_j^{(d)}), \Phi(\mathbf{x}_k^{(d')})) = 0$. Here $\Omega : \mathcal{X} \times \mathcal{X} \to \{0, 1\}$ is a *matching* function that is 1 for pairs of inputs across domains corresponding to the same object, and 0 otherwise.

However, just the above invariance will not work: we need the representation to be informative of the object O (otherwise even a constant Φ minimizes the above loss). Therefore, the second condition stipulates that X_C should be informative of the object, and hence about Y. We add the standard classification loss, leading to constrained optimization,

$$f_{\texttt{perfectmatch}} = \arg\min_{h,\Phi} \sum_{d=1}^{m} L_d(h(\Phi(X)), Y)$$
$$\texttt{s.t.} \sum_{\Omega(j,k)=1; d \neq d'} \text{dist}(\Phi(\mathbf{x}_j^{(d)}), \Phi(\mathbf{x}_k^{(d')})) = 0 \qquad (2)$$

where $L_d(h(\Phi(X), Y)) = \sum_{i=1}^{n_d} l(h(\Phi(\mathbf{x}_i^{(d)}), y_i^{(d)})$. Here f represents the composition $h \circ \Phi$. E.g., a neural network with $\Phi(x)$ as its rth layer, and h being the rest of the layers.

Note that there can be multiple $\Phi(\mathbf{x})$ (e.g., linear transformations) that are equally good for the prediction task. Since x_c is unidentifiable, we focus on the set of *stable* representations that are d-separated from D given O. Being independent of domain given the object, they cannot have any association with X_a, the high-level features that directly depend on domain (Figure 2b). The proof for the next theorem is in Suppl. B.5.

Theorem 1. *For a finite number of domains m, as the number of examples in each domain $n_d \to \infty$,*
1. The set of representations that satisfy the condition $\sum_{\Omega(j,k)=1; d \neq d'} \text{dist}(\Phi(\mathbf{x}_j^{(d)}), \Phi(\mathbf{x}_k^{(d')})) = 0$ contains the optimal $\Phi(\mathbf{x}) = X_C$ that minimizes the domain generalization loss in (1).
2. Assuming that $P(X_a | O, D) < 1$ for every high-level feature X_a that is directly caused by domain, and for P-admissible loss functions (Miller et al., 1993) whose minimization is conditional expectation (e.g., ℓ_2 or cross-entropy), a loss-minimizing classifier for the following loss is the true function f^*, for some value of λ.

$$f_{\texttt{perfectmatch}} = \arg\min_{h,\Phi} \sum_{d=1}^{m} L_d(h(\Phi(X)), Y) +$$
$$\lambda \sum_{\Omega(j,k)=1; d \neq d'} \text{dist}(\Phi(\mathbf{x}_j^{(d)}), \Phi(\mathbf{x}_k^{(d')})) \qquad (3)$$

4.4. Past work: Learning common representation

Using the SCM, we now compare the proposed invariance condition to domain-invariant and class-conditional domain-invariant objectives. d-separation results show that

both these objectives are incorrect: in particular, the class-conditional objective $\Phi(\mathbf{x}) \perp\!\!\!\perp D|Y$ is not satisfied by X_C, ($X_C \not\perp\!\!\!\perp D|Y_{true}$) due to a path through O. Even with infinite data across domains, they will not learn the true X_C. The proof is in Suppl. B.6.

Proposition 3. *The conditions enforced by domain-invariant ($\Phi(x) \perp\!\!\!\perp D$) or class-conditional domain-invariant ($\Phi(x) \perp\!\!\!\perp D|Y$) methods are not satisfied by the causal representation X_C. Thus, without additional assumptions, the set of representations that satisfy any of these conditions does not contain X_C, even as $n \to \infty$.*

5. MatchDG: Matching without objects

When object information is available, Eq. (3) provides a loss objective to build a classifer using causal features. However, object information is not always available, and in many datasets there may not be a perfect "counterfactual" match based on same object across domains. Therefore, we propose a two-phase, iterative contrastive learning method to approximate object matches.

The object-invariant condition from Section 4.2 can be interpreted as matching pairs of inputs from different domains that share the same X_C. To approximate it, our goal is to learn a matching $\Omega : \mathcal{X} \times \mathcal{X} \to \{0, 1\}$ such that pairs having $\Omega(\mathbf{x}, \mathbf{x}') = 1$ have low difference in $\mathbf{x}_c$ and $\mathbf{x}'_c$. We make the following assumption.

Assumption 1. *Let $(\mathbf{x}_i^{(d)}, y)$, $(\mathbf{x}_j^{(d')}, y)$ be any two points that belong to the same class, and let $(\mathbf{x}_k^{(d)} y')$ be any other point that has a different class label. Then the distance in causal features between $\mathbf{x}_i$ and $\mathbf{x}_j$ is smaller than that between $\mathbf{x}_i$ and $\mathbf{x}_k$ or $\mathbf{x}_j$ and $\mathbf{x}_k$: $\text{dist}(x_{c,i}^{(d)}, x_{c,j}^{(d')}) \leq \text{dist}(x_{c,i}^{(d)}, x_{c,k}^{(d')})$ and $\text{dist}(x_{c,j}^{(d)}, x_{c,i}^{(d')}) \leq \text{dist}(x_{c,j}^{(d)}, x_{c,k}^{(d')})$.*

5.1. Two-phase method with iterative matches

To learn a matching function Ω, we use unsupervised contrastive learning from (Chen et al., 2020; He et al., 2019) and adapt it to construct an iterative `MatchDG` algorithm that updates the both the representation and matches after each epoch. The algorithm relies on the property that two inputs from the same class have more similar causal features than inputs from different classes.

Contrastive Loss. To find matches, we optimize a contrastive representation learning loss that minimizes distance between same-class inputs from different domains in comparison to inputs from different classes across domains. Adapting the contrastive loss for a single domain (Chen et al., 2020), we consider *positive* matches as two inputs with the same class but different domains, and *negative* matches as pairs with different classes. For every positive match pair $(\mathbf{x}_j, \mathbf{x}_k)$, we propose a loss where τ is a hyperparameter, B is the batch size, and $\text{sim}(\mathbf{a}, \mathbf{b}) = \Phi(\mathbf{x}_a)^T \Phi(\mathbf{x}_b) / \|\Phi(\mathbf{x}_a)\| \|\Phi(\mathbf{x}_b)\|$ is the cosine similarity.

$$l(\mathbf{x}_j, \mathbf{x}_k) = -\log \frac{e^{\text{sim}(j,k)/\tau}}{e^{\text{sim}(j,k)/\tau} + \sum_{i=0, y_i \neq y_j}^{B} e^{\text{sim}(j,i)/\tau}} \quad (4)$$

Algorithm 1 MatchDG

In: Dataset $(d_i, x_i, y_i)_{i=1}^n$ from m domains, τ, t
Out: Function $f : \mathcal{X} \to \mathcal{Y}$
Create random match pairs Ω_Y.
Build a $p * q$ data matrix $\mathcal{M}$.
Phase I
while notconverged **do**
  for $batch \sim \mathcal{M}$ **do**
    Minimize contrastive loss (4).
  end for
  if epoch % t == 0 **then**
    Update match pairs using Φ_{epoch}.
  end if
end while
Phase II
Compute matching based on Φ.
Minimize the loss (3) with learnt match function Φ to obtain f.

Iterative matching. Our key insight is to update the positive matches during training. We start training with a random set of positive matches based on the classes, but after every t epochs, we update the positive matches based on the nearest same-class pairs in representation space and iterate until convergence. Hence for each anchor point, starting with an initial set of positive matches, in each epoch a representation is learnt using contrastive learning; after which the positive matches are themselves updated based on the closest same-class data points across domains in the representation. As a result, the method differentiates between data points of the same class instead of treating all of them as a single unit. With iterative updates to the positive matches, the aim is to account for intra-class variance across domains and match data points across domains that are more likely to share the same base object. In Suppl. D.6, we compare the gains due to the proposed iterative matching versus standard contrastive training.

Obtaining the final representation completes Phase I of the algorithm. In Phase II, we use this representation to compute a new match function based on closest same-class pairs and apply Eq. (3) to obtain a classifier regularized on those matches.

The importance of using two phases. We implement `MatchDG` as a 2-phase method, unlike previous methods (Motiian et al., 2017; Dou et al., 2019) that employed class-based contrastive loss as a regularizer with ERM. This is to avoid the classification loss interfering with the goal of learning an invariant representation across domains (e.g., in datasets where one of the domains has many more samples than others). Therefore, we first learn the match function

using only the contrastive loss. Our results in Suppl. D.4 show that the two-phase method provides better overlap with ground-truth perfect matches than optimizing classification and matching simultaneously.

To implement MatchDG we build a $p \times q$ data matrix containing $q-1$ positive matches for each input and then sample mini-batches from this matrix. The last layer of the contrastive loss network is considered as the learnt representation (see Algorithm 1; details are in Suppl. C.1).

5.2. MDG Hybrid

While MatchDG assumes no information about objects, it can be easily augmented to incorporate information about known objects. For example, in computer vision, a standard practice is to augment data by performing rotations, horizontal flips, color jitter, etc. These self-augmentations provide us with access to known objects, which can included as perfect-matches in MatchDG Phase-II by adding another regularizer to the loss from Eq 3. We name this method MDGHybrid and evaluate it alongside MatchDG for datasets where we can perform self augmentations.

6. Evaluation

We evaluate out-of-domain accuracy of MatchDG on two simulated benchmarks by Piratla et al. (2020), Rotated MNIST and Fashion-MNIST, on PACS dataset (Li et al., 2017), and on a novel Chest X-rays dataset. In addition, using the simulated datasets, we inspect the quality of matches learnt by MatchDG by comparing them to ground-truth object-based matches. For PACS and Chest X-rays, we also implement MDGHybrid that uses augmentations commonly done while training neural networks. We compare to 1) ERM: Standard empirical risk minimization, 2) ERM-RandMatch that implements the loss from Eq. (3) but with randomly selected matches from the same class (Motiian et al., 2017), 3) other state-of-the-art methods for each dataset. For all matching-based methods, we use the cross-entropy loss for L_d and ℓ_2 distance for dist in Eq.(3). Details of implementation and the datasets are in Suppl. C.1. All the numbers are averaged over 3 runs with standard deviation in brackets.

Rotated MNIST & Fashion-MNIST. The datasets contain rotations of grayscale MNIST handwritten digits and fashion article images from 0° to 90° with an interval of 15° (Ghifary et al., 2015), where each rotation angle represents a domain and the task is to predict the class label. Since different domains' images are generated from the same base image (object), there exist perfect matches across domains. Following CSD, we report accuracy on 0° and 90° together as the test domain and the rest as the train domains; since these test angles, being extreme, are the hardest to generalize to (standard setting results are in Suppl. D.1, D.2).

PACS. This dataset contains total 9991 images from four domains: Photos (P), Art painting (A), Cartoon (C) and Sketch (S). The task is to classify objects over 7 classes. Following (Dou et al., 2019), we train 4 models with each domain as the target using Resnet-18, Resnet-50 and Alexnet.

Chest X-rays. We introduce a harder real-world dataset based on Chest X-ray images from three different sources: NIH (Wang et al., 2017), ChexPert (Irvin et al., 2019) and RSNA (rsn, 2018). The task is to detect whether the image corresponds to a patient with Pneumonia (1) or not (0). To create spurious correlation, all images of class 0 in the training domains are translated vertically downwards; while no such translation is done for the test domain.

Model Selection. While using a validation set from the test domain may improve classification accuracy, it goes against the problem motivation of generalization to unseen domains. Hence, we use only data from source domains to construct a validation set (except when explicitly mentioned in Table 4, to compare to past methods that use test domain validation).

6.1. Rotated MNIST and Fashion MNIST

Table 2 shows classification accuracy on rotMNIST and rotFashionMNIST for test domains 0° & 90° using Resnet-18 model. On both datasets, MatchDG *outperforms* all baselines. The last column shows the accuracy for an oracle method, ERM-PerfMatch that has access to ground-truth perfect matches across domains. MatchDG's accuracy lies between ERM-RandMatch and ERM-PerfMatch, indicating the benefit of learning a matching function. As the number of training domains decrease, the gap between MatchDG and baselines is highlighted: with 3 source domains for rotFashionMNIST, MatchDG achieves accuracy of 43.8% whereas the next best method ERM-RandMatch achieves 38.4%.

We also evaluate on a simpler 2-layer LeNet (Motiian et al., 2017), and the model from (Gulrajani & Lopez-Paz, 2020) to compare MatchDG to prior works (Ilse et al., 2020; Ganin et al., 2016; Shankar et al., 2018; Goodfellow et al., 2014); the results are in Suppl. D.1, D.2.

Why MatchDG works? We compare the matches returned by MatchDG Phase I (on Resnet-18 network) to the ground-truth perfect matches and find that it has significantly higher overlap than matching based on ERM loss (Table 3). We report three metrics on the representation learnt: percentage of MatchDG matches that are perfect matches, %-age of inputs for which the perfect match is within the top-10 ranked MatchDG matches, and mean rank of perfect matches measured by distance over the MatchDG representation.

On all three metrics, MatchDG finds a representation whose

Table 2. Accuracy for Rotated MNIST & Fashion-MNIST datasets on target domains of 0° and 90°. Accuracy for CSD (Piratla et al., 2020), MASF (Dou et al., 2019), IRM (Arjovsky et al., 2019) are reproduced from their code. Results for the other versions of Rotated MNIST with all test angles (LetNet (Motiian et al., 2017), DomainBed (Gulrajani & Lopez-Paz, 2020)) are in Suppl. D.1, D.2.

Dataset	Source	ERM	MASF	CSD	IRM	RandMatch	MatchDG	PerfMatch (Oracle)
Rotated MNIST	15, 30, 45, 60, 75	93.0 (0.11)	93.2 (0.2)	94.5 (0.35)	92.8 (0.53)	93.4 (0.26)	**95.1** (0.25)	96.0 (0.41)
	30, 45, 60	76.2 (1.27)	69.4 (1.32)	77.7 (1.88)	75.7 (1.11)	78.3 (0.55)	**83.6** (1.44)	89.7 (1.68)
	30, 45	59.7 (1.75)	60.8 (1.53)	62.0 (1.31)	59.5 (2.61)	63.8 (3.92)	**69.7** (1.30)	80.4 (1.79)
Rotated Fashion MNIST	15, 30, 45, 60, 75	77.9 (0.13)	72.4 (2.9)	78.7 (0.38)	77.8 (0.02)	77.0 (0.42)	**80.9** (0.26)	81.6 (0.46)
	30, 45, 60	36.1 (1.91)	29.7 (1.73)	36.3 (2.65)	37.8 (1.85)	38.4 (2.73)	**43.8** (1.33)	54.0 (2.79)
	30, 45	26.1 (1.10)	22.8 (1.26)	24.2 (1.69)	26.6 (1.06)	26.9 (0.34)	**33.0** (0.72)	41.8 (1.78)

Table 3. Overlap with perfect matches. top-10 overlap and the mean rank for perfect matches for MatchDG and ERM over all training domains. Lower is better for mean rank.

Dataset	Method	Overlap (%)	Top 10 Overlap (%)	Mean Rank
MNIST	ERM	15.8 (0.42)	48.8 (0.78)	27.4 (0.89)
	MatchDG (Default)	**28.9** (1.24)	**64.2** (2.42)	**18.6** (1.59)
	MatchDG (PerfMatch)	47.4 (2.25)	83.8 (1.46)	6.2 (0.61)
Fashion MNIST	ERM	2.1 (0.12)	11.1 (0.63)	224.3 (8.73)
	MatchDG (Default)	**17.9** (0.62)	**43.1** (0.83)	**89.0** (3.15)
	MatchDG (PerfMatch)	56.2 (1.79)	87.2 (1.48)	7.3 (1.18)

matches are more consistent with ground-truth perfect matches. For both rotMNIST and rotFashionMNIST datasets, about 50% of the inputs have their perfect match within top-10 ranked matches based on the representation learnt by MatchDG Phase I. About 25% of all matches learnt by MatchDG are perfect matches. For comparison, we also show metrics for an (oracle) MatchDG method that is initialized with perfect matches: it achieves better overall and Top-10 values. Similar results for MatchDG Phase 2 are in Suppl. D.4. Mean rank for rotFashionMNIST may be higher because of the larger sample size $10,000$ per domain; metrics for training with 2000 samples are in Suppl. D.5. To see how the overlap with perfect matches affects accuracy, we simulate random matches with 25%, 50% and 75% overlap with perfect matches (Suppl. Tbl. D.3). Accuracy increases with the fraction of perfect matches, indicating the importance of capturing good matches.

MatchDG vs. IRM on zero training error. Since neural networks often achieve zero training error, we also evaluate the effectiveness of the MatchDG regularization under this regime. Fig. 3 shows the matching loss term as training proceeds for rotMNIST and rotFashionMNIST. Even

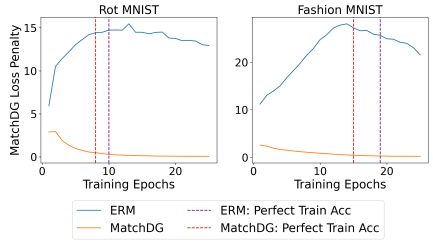

(a) MatchDG Penalty during training

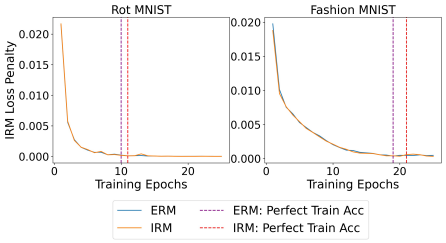

(b) IRM Penalty during training

Figure 3. MatchDG regularization penalty is not trivially minimized even as the training error goes to zero.

after the model achieves zero training error, we see that plain ERM objective is unable to minimize the matching loss (and thus MatchDG penalty is needed). This is because MatchDG regularization depends on comparing the (last layer) representations, and zero training error does not mean that the representations within each class are the same. In contrast, regularizations that are based on comparing loss between training domains such as the IRM penalty can be satisfied by plain ERM as the training error goes to zero (Fig. 3(b)); similar to Fig. (5) from (Krueger et al., 2020) where ERM can minimize IRM penalty on Colored MNIST.

6.2. PACS dataset

ResNet-18. On the PACS dataset with ResNet-18 architecture (Table 4), our methods are competitive to state-of-the-

Table 4. Accuracy on PACS with ResNet 18 (default), and Resnet 18 with test domain validation. The results for JiGen (Carlucci et al., 2019), DDAIG (Zhou et al., 2020), SagNet (Nam et al., 2019), DDEC (Asadi et al., 2019), were taken from the DomainBed (Gulrajani & Lopez-Paz, 2020) paper. For G2DM (Albuquerque et al., 2020a), CSD (Piratla et al., 2020), RSC (Huang et al., 2020) it was taken from the respective paper. Extensive comparison with other works and std. dev. in results is in Supp E.1.

	P	A	C	S	Average.
ERM	95.38	77.68	78.98	74.75	81.70
JiGen	96.0	79.42	75.25	71.35	80.41
G2DM	93.75	77.78	75.54	77.58	81.16
CSD	94.1	78.9	75.8	76.7	81.4
DDAIG	95.30	**84.20**	78.10	74.70	83.10
SagNet	95.47	83.58	77.66	76.30	83.25
DDEC	**96.93**	83.01	79.39	78.62	84.46
RSC	95.99	83.43	80.31	**80.85**	**85.15**
RandMatch	95.37	78.16	78.83	75.13	81.87
MatchDG	95.93	79.77	80.03	77.11	83.21
MDGHybrid	96.15	81.71	**80.75**	78.79	84.35
G2DM (Test)	94.63	81.44	79.35	79.52	83.34
RandMatch (Test)	95.57	79.09	79.37	77.60	82.91
MatchDG (Test)	96.53	81.32	80.70	79.72	84.56
MDGHybrid (Test)	**96.67**	**82.80**	**81.61**	**81.05**	**85.53**

Table 5. Accuracy on PACS with architecture ResNet 50. The results for IRM (Arjovsky et al., 2019), CORAL (Sun & Saenko, 2016), were taken from the DomainBed (Gulrajani & Lopez-Paz, 2020) paper. The result for RSC (Huang et al., 2020) was taken from their paper. Comparison with other works in Supp E.1.

	P	A	C	S	Average.
DomainBed (ResNet50)	97.8	**88.1**	77.9	79.1	85.7
IRM (ResNet50)	96.7	85.0	77.6	78.5	84.4
CORAL (ResNet50)	97.6	87.7	79.2	79.4	86.0
RSC (ResNet50)	97.92	87.89	82.16	**83.35**	**87.83**
RandMatch (ResNet50)	97.89	82.16	81.68	80.45	85.54
MatchDG (ResNet50)	97.94	85.61	82.12	78.76	86.11
MDGHybrid (ResNet50)	**98.36**	86.74	**82.32**	82.66	87.52

art results averaged over all domains. The MDGHybrid has the highest average accuracy across domains, except compared to DDEC and RSC. These works do not disclose their model selection strategy (whether the results are using source or test domain validation). Therefore, we also report results of MatchDG and MDGHybrid using test domain validation, where MDGHybrid obtains comparable results to the best-performing method. In addition, with DDEC (Asadi et al., 2019), it is not a fair comparison since they use additional style transfer data from Behance BAM! dataset during training.

ResNet-50. We implement MatchDG on Resnet50 model (Table 5) used by the ERM in DomainBed. Adding MatchDG loss regularization improves the accuracy of DomainBed, from 85.7 to 87.5 with MDGHybrid. Also, MDGHybrid performs better than the prior approaches using Resnet50 architecture, except RSC (Huang et al., 2020), whose results (87.83) are close to ours (87.52). Note that we chose a subset of the best-performing baselines for Table 4, 5; an extensive comparison with other works is in Suppl. E.1. Suppl. E.2 gives the results using AlexNet network, and a t-SNE plot (Figure 5) to show the quality of representation learnt by MatchDG.

Table 6. Chest X-Rays data. As an upper bound, training ERM on the target domain itself yields 73.8%, 66.5%, and 59.9% accuracy for RSNA, ChexPert, and NIH respectively.

	RSNA	ChexPert	NIH
ERM	55.1 (2.93)	60.9 (0.51)	53.4 (1.36)
IRM	57.0 (0.75)	63.3 (0.25)	54.6 (0.88)
CSD	58.6 (1.63)	**64.4 (0.88)**	54.7 (0.13)
RandMatch	56.3 (3.38)	55.3 (2.25)	53.1 (0.13)
MatchDG	58.2 (1.25)	59.0 (0.25)	53.2 (0.65)
MDGHybrid	**64.3** (0.75)	60.6 (0.25)	**57.6** (0.13)

6.3. Chest X-rays dataset

Table 6 provides results for the Chest X-rays dataset, where the spurious correlation of vertical translation with the class label in source domains may lead the models to learn an unstable relationship. With RSNA as the target domain, ERM obtains 79.8%, 81.8% accuracy on the source domains while its accuracy drops to 55.1% for the target domain. In contrast, MDGHybrid obtain the highest classification accuracy (8 % above ERM), followed by CSD and MatchDG; while methods like ERM and IRM are more susceptible to spurious correlation. However, on ChexPert as the target domain, CSD and IRM do better than ERM while matching-based methods are not effective. We conjecture these varying trends might be due to the inherent variability in images in the source domains, indicating the challenges of building domain generalization methods for real-world datasets.

7. Conclusion

We presented a causal view of domain generalization that provides an object-conditional objective. Simple matching-based methods perform competitively to state-of-the-art methods on PACS, indicating the importance of choosing the right invariance. The proposed MatchDG uses certain assumptions when objects are unknown. More work needs to be done to develop better matching methods, as indicated by the mixed results on the Chest-Xrays dataset.

Acknowledgements. We would like to thank Adith Swaminathan, Aditya Nori, Emre Kiciman, Praneeth Netrapalli, Tobias Schnabel, Vineeth Balasubramanian and the reviewers who provided us valuable feedback on this work. We also thank Vihari Piratla who helped us with reproducing the CSD method and other baselines.

References

Kaggle: Rsna pneumonia detection challenge, 2018. URL https://www.kaggle.com/c/rsna-pneumonia-detection-challenge .

Ahuja, K., Shanmugam, K., Varshney, K., and Dhurandhar, A. Invariant risk minimization games. arXiv preprint arXiv:2002.04692, 2020.

Akuzawa, K., Iwasawa, Y., and Matsuo, Y. Adversarial invariant feature learning with accuracy constraint for domain generalization. In Joint European Conference on Machine Learning and Knowledge Discovery in Databases, pp. 315–331. Springer, 2019.

Albuquerque, I., Monteiro, J., Darvishi, M., Falk, T. H., and Mitliagkas, I. Generalizing to unseen domains via distribution matching, 2020a.

Albuquerque, I., Naik, N., Li, J., Keskar, N., and Socher, R. Improving out-of-distribution generalization via multi-task self-supervised pretraining. arXiv preprint arXiv:2003.13525, 2020b.

Arjovsky, M., Bottou, L., Gulrajani, I., and Lopez-Paz, D. Invariant risk minimization. arXiv preprint arXiv:1907.02893, 2019.

Asadi, N., Sar , A. M., Hosseinzadeh, M., Karimpour, Z., and Eftekhari, M. Towards shape biased unsupervised representation learning for domain generalization. arXiv preprint arXiv:1909.08245, 2019.

Balaji, Y., Sankaranarayanan, S., and Chellappa, R. Metareg: Towards domain generalization using meta-regularization. In Advances in Neural Information Processing Systems, pp. 998–1008, 2018.

Carlucci, F. M., D'Innocente, A., Bucci, S., Caputo, B., and Tommasi, T. Domain generalization by solving jigsaw puzzles. In Proceedings of the IEEE Conference on Computer Vision and Pattern Recognition, pp. 2229–2238, 2019.

Chen, T., Kornblith, S., Norouzi, M., and Hinton, G. A simple framework for contrastive learning of visual representations. arXiv preprint arXiv:2002.05709, 2020.

Christiansen, R., P ster, N., Jakobsen, M. E., Gnecco, N., and Peters, J. A causal framework for distribution generalization. arXiv e-prints, pp. arXiv–2006, 2020.

Cohen, J. P., Hashir, M., Brooks, R., and Bertrand, H. On the limits of cross-domain generalization in automated x-ray prediction. arXiv preprint arXiv:2002.02497, 2020.

Dou, Q., de Castro, D. C., Kamnitsas, K., and Glocker, B. Domain generalization via model-agnostic learning of semantic features. In Advances in Neural Information Processing Systems, pp. 6447–6458, 2019.

D'Innocente, A. and Caputo, B. Domain generalization with domain-speci c aggregation modules. In German Conference on Pattern Recognition, pp. 187–198. Springer, 2018.

Ganin, Y., Ustinova, E., Ajakan, H., Germain, P., Larochelle, H., Laviolette, F., Marchand, M., and Lempitsky, V. Domain-adversarial training of neural networks. The Journal of Machine Learning Research, 17(1):2096–2030, 2016.

Ghifary, M., Bastiaan Kleijn, W., Zhang, M., and Balduzzi, D. Domain generalization for object recognition with multi-task autoencoders. In Proceedings of the IEEE international conference on computer vision, pp. 2551–2559, 2015.

Ghifary, M., Balduzzi, D., Kleijn, W. B., and Zhang, M. Scatter component analysis: A uni ed framework for domain adaptation and domain generalization. IEEE transactions on pattern analysis and machine intelligence, 39(7):1414–1430, 2016.

Gong, M., Zhang, K., Liu, T., Tao, D., Glymour, C., and Schölkopf, B. Domain adaptation with conditional transferable components. In International conference on machine learning, pp. 2839–2848, 2016.

Goodfellow, I. J., Shlens, J., and Szegedy, C. Explaining and harnessing adversarial examples. arXiv preprint arXiv:1412.6572, 2014.

Gulrajani, I. and Lopez-Paz, D. In search of lost domain generalization. arXiv preprint arXiv:2007.01434, 2020.

He, K., Fan, H., Wu, Y., Xie, S., and Girshick, R. Momentum contrast for unsupervised visual representation learning. arXiv preprint arXiv:1911.05722, 2019.

Heinze-Deml, C. and Meinshausen, N. Conditional variance penalties and domain shift robustness. arXiv preprint arXiv:1710.11469, 2019.

Hu, S., Zhang, K., Chen, Z., and Chan, L. Domain generalization via multidomain discriminant analysis. In Uncertainty in arti cial intelligence: proceedings of the... conference. Conference on Uncertainty in Arti cial Intelligence, volume 35. NIH Public Access, 2019.

Huang, Z., Wang, H., Xing, E. P., and Huang, D. Self-challenging improves cross-domain generalization. arXiv preprint arXiv:2007.02454, 2020.

Ilse, M., Tomczak, J. M., Louizos, C., and Welling, M. Diva: Domain invariant variational autoencoders. Medical Imaging with Deep Learning, pp. 322–348. PMLR, 2020.

Irvin, J., Rajpurkar, P., Ko, M., Yu, Y., Ciurea-Ilcus, S., Chute, C., Marklund, H., Haghgoo, B., Ball, R., Shpanskaya, K., et al. Chexpert: A large chest radiograph dataset with uncertainty labels and expert comparison. In Proceedings of the AAAI Conference on Arti cial Intelligence, volume 33, pp. 590–597, 2019.

Johansson, F. D., Sontag, D., and Ranganath, R. Support and invertibility in domain-invariant representations. The 22nd International Conference on Arti cial Intelligence and Statistics, pp. 527–536, 2019.

Krueger, D., Caballero, E., Jacobsen, J.-H., Zhang, A., Binas, J., Priol, R. L., and Courville, A. Out-of-distribution generalization via risk extrapolation (rex). arXiv preprint arXiv:2003.00688, 2020.

Li, D., Yang, Y., Song, Y.-Z., and Hospedales, T. M. Deeper, broader and artier domain generalization. In Proceedings of the IEEE international conference on computer vision, pp. 5542–5550, 2017.

Li, D., Yang, Y., Song, Y.-Z., and Hospedales, T. M. Learning to generalize: Meta-learning for domain generalization. In Thirty-Second AAAI Conference on Arti cial Intelligence, 2018a.

Li, D., Zhang, J., Yang, Y., Liu, C., Song, Y.-Z., and Hospedales, T. M. Episodic training for domain generalization. In Proceedings of the IEEE International Conference on Computer Vision, pp. 1446–1455, 2019a.

Li, D., Yang, Y., Song, Y.-Z., and Hospedales, T. Sequential learning for domain generalization. arXiv preprint arXiv:2004.01377, 2020.

Li, H., Jialin Pan, S., Wang, S., and Kot, A. C. Domain generalization with adversarial feature learning. In Proceedings of the IEEE Conference on Computer Vision and Pattern Recognition, pp. 5400–5409, 2018b.

Li, Y., Gong, M., Tian, X., Liu, T., and Tao, D. Domain generalization via conditional invariant representations. In Thirty-Second AAAI Conference on Arti cial Intelligence, 2018c.

Li, Y., Tian, X., Gong, M., Liu, Y., Liu, T., Zhang, K., and Tao, D. Deep domain generalization via conditional invariant adversarial networks. In Proceedings of the European Conference on Computer Vision (ECCV), pp. 624–639, 2018d.

Li, Y., Yang, Y., Zhou, W., and Hospedales, T. M. Feature-critic networks for heterogeneous domain generalization. arXiv preprint arXiv:1901.11448, 2019b.

Maaten, L. v. d. and Hinton, G. Visualizing data using t-sne. Journal of machine learning research, 9(Nov): 2579–2605, 2008.

Magliacane, S., van Ommen, T., Claassen, T., Bongers, S., Versteeg, P., and Mooij, J. M. Domain adaptation by using causal inference to predict invariant conditional distributions. In Advances in Neural Information Processing Systems, pp. 10846–10856, 2018.

Matsuura, T. and Harada, T. Domain generalization using a mixture of multiple latent domains. In AAAI, pp. 11749–11756, 2020.

Miller, J. W., Goodman, R., and Smyth, P. On loss functions which minimize to conditional expected values and posterior probabilities. IEEE Transactions on Information Theory, 39(4):1404–1408, 1993.

Motiian, S., Piccirilli, M., Adjeroh, D. A., and Doretto, G. Uni ed deep supervised domain adaptation and generalization. In Proceedings of the IEEE International Conference on Computer Vision, pp. 5715–5725, 2017.

Muandet, K., Balduzzi, D., and Schölkopf, B. Domain generalization via invariant feature representation. In International Conference on Machine Learning, pp. 10–18, 2013.

Nam, H., Lee, H., Park, J., Yoon, W., and Yoo, D. Reducing domain gap via style-agnostic networks. arXiv preprint arXiv:1910.11645, 2019.

Pearl, J. Causality. Cambridge university press, 2009.

Peters, J., Bühlmann, P., and Meinshausen, N. Causal inference by using invariant prediction: identi cation and con dence intervals. Journal of the Royal Statistical Society: Series B (Statistical Methodology), 78(5):947–1012, 2016.

Piratla, V., Netrapalli, P., and Sarawagi, S. Ef cient domain generalization via common-speci c low-rank decomposition. Proceedings of the International Conference of Machine Learning (ICML) 2020, 2020.

Rahman, M. M., Fookes, C., Baktashmotlagh, M., and Sridharan, S. Correlation-aware adversarial domain adaptation and generalization. Pattern Recognition, 100:107124, 2020.

Rojas-Carulla, M., Schölkopf, B., Turner, R., and Peters, J. Invariant models for causal transfer learning. The Journal of Machine Learning Research, 19(1):1309–1342, 2018.

Sagawa, S., Koh, P. W., Hashimoto, T. B., and Liang, P. Distributionally robust neural networks for group shifts: On the importance of regularization for worst-case generalization. arXiv preprint arXiv:1911.08731, 2019.

Shah, H., Tamuly, K., Raghunathan, A., Jain, P., and Netrapalli, P. The pitfalls of simplicity bias in neural networks. arXiv preprint arXiv:2006.07710, 2020.

Shankar, S., Piratla, V., Chakrabarti, S., Chaudhuri, S., Jyothi, P., and Sarawagi, S. Generalizing across domains via cross-gradient training. In International Conference on Learning Representations, 2018.

Sun, B. and Saenko, K. Deep coral: Correlation alignment for deep domain adaptation. In European conference on computer vision, pp. 443–450. Springer, 2016.

Volpi, R., Namkoong, H., Sener, O., Duchi, J. C., Murino, V., and Savarese, S. Generalizing to unseen domains via adversarial data augmentation. In Advances in Neural Information Processing Systems, pp. 5334–5344, 2018.

Wang, H., He, Z., Lipton, Z. C., and Xing, E. P. Learning robust representations by projecting superficial statistics out. arXiv preprint arXiv:1903.06256, 2019.

Wang, X., Peng, Y., Lu, L., Lu, Z., Bagheri, M., and Summers, R. M. Chestx-ray8: Hospital-scale chest x-ray database and benchmarks on weakly-supervised classification and localization of common thorax diseases. In Proceedings of the IEEE conference on computer vision and pattern recognition, pp. 2097–2106, 2017.

Wang, Y., Li, H., and Kot, A. C. Heterogeneous domain generalization via domain mixup. In ICASSP 2020-2020 IEEE International Conference on Acoustics, Speech and Signal Processing (ICASSP), pp. 3622–3626. IEEE, 2020.

Xu, M., Zhang, J., Ni, B., Li, T., Wang, C., Tian, Q., and Zhang, W. Adversarial domain adaptation with domain mixup. arXiv preprint arXiv:1912.01805, 2019.

Yan, S., Song, H., Li, N., Zou, L., and Ren, L. Improve unsupervised domain adaptation with mixup training. arXiv preprint arXiv:2001.00677, 2020.

Zhao, H., Combes, R. T. d., Zhang, K., and Gordon, G. J. On learning invariant representation for domain adaptation. arXiv preprint arXiv:1901.09453, 2019.

Zhao, S., Gong, M., Liu, T., Fu, H., and Tao, D. Domain generalization via entropy regularization. In Advances in Neural Information Processing Systems, 33, 2020.

Zhou, K., Yang, Y., Hospedales, T. M., and Xiang, T. Deep domain-adversarial image generation for domain generalisation. In AAAI, pp. 13025–13032, 2020.

A. Synthetic Data (Slab Dataset and Simple Counter-example)

A.1. Implementation Details for the Slab Dataset

Dataset The synthetic slab dataset (Section 3.2) consists of a binary label y and 2-dimensional features; one feature has a linear relationship with y while the other has a more complex "slab" relationship with y. The features vary in their simplicity, a measure of the simplicity of the feature is given by the number of linear pieces in the optimal classification/decision curve (Figure 1, (Shah et al., 2020)). Hence, the linear features are simpler as they only have 1 linear piece in the optimal decision boundary, as opposed to the slab features that have k linear pieces in the piecewise linear optimal decision boundary.

The synthetic slab dataset was introduced for detecting simplicity bias in neural networks (Shah et al., 2020), to demonstrate that neural networks trained with SGD learn the simpler linear feature as opposed to the slab feature. We extend this dataset for the domain generalization (DG) task, by making the linear block features spurious due to domain dependent noise addition as described below. The effect of the slab feature on y remains the same across domains. Presence of the spurious linear feature should enable an ideal DG algorithm to differentiate it from the stable slab feature, and break the simplicity bias in neural networks. However, the invariance introduced by different DG methods can have a big impact. Using this dataset, we show that the class-conditional distribution matching constraint is not sufficient (section 3.2); it is possible to satisfy the constraint using the spurious linear feature too.

The linear block features contain the positive (y=1) and the negative (y=0) labels sampled from uniform distributions $U(0.1, 1.0)$ and $U(-1.0, -0.1)$ respectively. To make the linear features spurious, we add noise to the linear features s.t. data points are sampled from $U(-0.1, 0.1)$ with probability p, and sampled from $U(0.1, 1.0)$ (y=1) or $U(-1.0, -0.1)$ (y=0) with probability $1-p$. The k-slab feature ranges from [-1, 1] and within it has different "slabs" corresponding to uniform distributions of the feature's value, conditioned on class label y. The labels for these slabs alternate between positive (y=1) and negative (y=0) as the numeric value of the slab feature increases. The length for each slab is given by $\frac{2-m(k-1)}{k}$ where k is the total number of slabs, and m is the margin between two slabs.

Linear Block Feature:

$$p_l(x|y=0) = \begin{cases} U(-0.1, 0.1) & \text{with prob. } p \\ U(-1.0, -0.1) & \text{with prob. } 1-p \end{cases}$$

$$p_l(x|y=1) = \begin{cases} U(-0.1, 0.1) & \text{with prob. } p \\ U(0.1, 1.0) & \text{with prob. } 1-p \end{cases}$$

Slab Block Feature:

Let k be the total number of slabs, and m be the margin between two slabs.

Slab length: $L = \frac{2-m(k-1)}{k}$

Start index: $l(i) = -1 + iL$

$$p_s(x|y=0) = U(l(i), l(i)+L) \quad \text{for } i \in \{0, 2, 4, \ldots\}$$

$$p_s(x|y=1) = U(l(i), l(i)+L) \quad \text{for } i \in \{1, 3, 5, \ldots\}$$

We also a constant (domain independent) noise to the relationship between the slab feature and the class label by flipping the original label with probability p_s.

Source and Target Domains We generate two source data domains with noise probabilities as 0.0 and 0.1, and generate the target domain with complete noise i.e. 1.0, rendering the linear block feature not informative of the label in the target domain. However, the slab block features have a stable relationship with the labels across the multiple source and target domains. We choose $k = 7$, $m = 0.1$, and $p_s = 0.1$ for the slab block features in our experiments. We sample 1k data points per domain, which leads to 2k training data points (source domain with p_l as 0.0 and 0.1), and 1k test data points (target domain with p_l as 1.0). Also, for hyperparameter tuning (model selection), we sample additional 250 data points per source domain as the validation set.

Model Architecture The overall architecture consists of a representation network along with a classification network, detailed below. Input Dim refers to the input data dimension, which is 2 dimensional (linear block feature, slab block feature). Num Classes refers to the total number of output classes, which is binary classification for the synthetic slab dataset. We refer a fully connected dense layer by FC layer, with the input and output dimensions for that layer in brackets.

Representation Network

- FC layer: (Input Dim, 100)
- ReLU activation

Classification Network

- FC layer: (100, 100)

Table 7. Hyper parameter selection details for the slab dataset. We mention the Optimal Value for each hyper parameter and the Range used for grid search. We leave the optimal value for Epochs as blank since we do early stopping based on the validation loss, with the total number of epochs for each model as 100.

Method	Hyper Parameter	Optimal Value	Range
DANN	Lambda	0.01	[0.01, 0.1, 1.0, 10.0, 100.0]
	Gradient Penalty	0.1	[0.01, 0.1, 1.0, 10.0]
	Discriminator Steps	4	[1, 2, 4, 8]
CDANN	Lambda	0.01	[0.01, 0.1, 1.0, 10.0, 100.0]
	Gradient Penalty	1.0	[0.01, 0.1, 1.0, 10.0]
	Discriminator Steps	2	[1, 2, 4, 8]
MMD	Lambda	0.1	[0.1, 1.0, 10.0]
C-MMD	Lambda	0.1	[0.1, 1.0, 10.0]
CORAL	Lambda	0.1	[0.1, 1.0, 10.0]
C-CORAL	Lambda	0.1	[0.1, 1.0, 10.0]
RandMatch	Lambda	1.0	[0.1, 1.0, 10.0]
PerfMatch	Lambda	1.0	[0.1, 1.0, 10.0]

- FC layer: (100, Num Classes)

For methods like DANN (Ganin et al., 2016), and CDAAN (Li et al., 2018d), which also require domain discriminators, we use the same architecture for them as that of the classification network.

Methods We use Cross-Entropy for the classification loss in ERM and all the other methods. The regularization penalty of all the methods is placed on the output of the representation network.

For the methods DANN (Ganin et al., 2016), CDANN (Li et al., 2018d), MMD (Li et al., 2018b), CORAL (Sun & Saenko, 2016), we used their implementation available in DomainBed (Gulrajani & Lopez-Paz, 2020). We extended the implementation of MMD and CORAL from DomainBed to their class conditional versions, C-MMD, and C-CORAL. The extension to class conditional version was done by computing their respective penalty over domains conditioned on a particular class label.

For RandMatch (Motiian et al., 2017) and PerfMatch, we use l_2 distance for dist in (Eq: 3). The match function Ω in the RandMatch algorithm is defined as randomly matching any two data points across domains with the same class label. For the PerfMatch algorithm, the match function Ω accepts two data points across domains with the same slab id as valid matches (the slab id corresponds to the value of the causal feature: two inputs with the same slab id have similar causal features).

Note on method selection Our objective with the synthetic slab dataset is to compare the performance of conditional distribution matching (CDM) methods to that of Perfect Match. We chose the above mentioned CDM methods for experimentation since the other CDM methods (Li et al., 2018c; Ghifary et al., 2016; Hu et al., 2019) mentioned in the related works (Section 2, main paper) did not have their implementation publicly available. We found the implementation of CDANN (Li et al., 2018d) in the DomainBed (Gulrajani & Lopez-Paz, 2020) repository, which also provided implementation for the unconditional distribution matching methods like MMD (Li et al., 2018b), and CORAL (Sun & Saenko, 2016). Hence, we extended MMD and CORAL to their class-conditional variant using their original implementation from the DomainBed repository.

Hyperparameter Tuning All the methods were trained using SGD, with batch size 128, learning rate 0.1 and weight decay 5e-4. We train each method for 100 epochs and do early stopping based on the validation loss.

Further details regarding the tuning of hyperparameters specific to each method's regularization technique are provided in Table 7. The loss objective of all the methods can be written as ERM + λ*Regularization Penalty; and we provide the optimal values and grid range for the hyperparam λ in Table 7. Also, some methods like DANN, C-DANN have additional hyperparams, which are specified in the same table. The grid search range for methods that were implemented using DomainBed (Gulrajani & Lopez-Paz, 2020) is taken from the Table 8 in the DomainBed paper.

A.2. Simple counter-example and its relationship to the MatchDG assumption.

The `MatchDG` method depends on Assumption 1 (Section 5) which requires that same-class inputs across domains are closer in causal features than different-class inputs. Note

that the example in Section 3.1 does not satisfy this assumption. However, there exist many variations of the setup that do follow the MatchDG assumption, and still class-conditional methods cannot recover the true causal feature. For instance, by setting $|x_c'| = |x_c| + \kappa$ where $\kappa > 1.5$ and $\alpha_1 = \kappa + 1, \alpha_2 = \kappa + 2$ for domain 1 and domain 2 respectively, the train domains satisfy the MatchDG assumption.

Overall, the goal of the simple example in Section 3.1 is to show that there exist datasets where class-conditional methods would not work, but Perfect-Match does. MatchDG's assumption works in a subset of these datasets. In future work, matching-based methods can be developed that relax the MatchDG assumption.

B. Theory and Proofs

B.1. Constructing the causal graph

When considering classification tasks, there are two viewpoints on whether the features cause the class label, or whether the class labels cause the features. (Gong et al., 2016; Magliacane et al., 2018; Rojas-Carulla et al., 2018) assume a generative process where the true class label determines the features in the observed data. In contrast, (Peters et al., 2016; Arjovsky et al., 2019) consider a generative process where the features are used to assign a label, e.g., when manually labelling a set of images. We believe that both mechanisms are possible, depending on the context. In particular, it is plausible that the true class label Y_{true} causes the features, but it is not observed. Instead, what is observed is the output of a manual labelling process, where the features are used to label each input with its class Y (Arjovsky et al., 2019).

Given these differences, we construct a causal graph (Figure 2) that includes both Y_{true} and Y (as in (Heinze-Deml & Meinshausen, 2019)), and is consistent with both viewpoints about the direction of the causal mechanism. Importantly, all d-separation results reported in the main text hold true irrespective of whether we choose Y or Y_{true} as the class label. We use Y as the label in the main text, since it corresponds to many settings where the observed class label is a result of a (possibly noisy) manual labelling process.

In addition, we chose to represent X_C and X_A as near-to-final features, that are combined using a simple operation to generate the observed features X. Under this representation, the object O does cause X_A; X_A is produced by combination of the domain and the object. Another equally valid construction is to assume that X_A contains only the domain information, and a more complex operation generates the observed features using X_C (object information) and X_A. The corresponding causal graph will omit the edge from object O to X_A. Both these graphs are allowed by our framework. All d-separation results reported in the main text hold true irrespective of whether there exists an edge from O to X_A.

B.2. D-separation

We first expand on the d-separation definition, providing a few examples that illustrate conditional independence implications of specific graph structures in Figure 4. We use these three conditions for the proofs below.

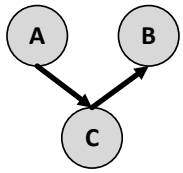

(a) Chain: $A \not\perp\!\!\!\perp B; A \perp\!\!\!\perp B|C$

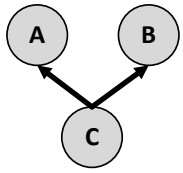

(b) Fork: $A \not\perp\!\!\!\perp B; A \perp\!\!\!\perp B|C$

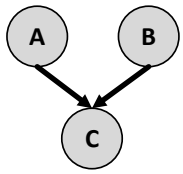

(c) Collider: $A \perp\!\!\!\perp B; A \not\perp\!\!\!\perp B|C$

Figure 4. Causal graphs with the node C as a chain, fork, or a collider. By the d-separation criteria, A and B are conditionally independent given C in (a) and (b). In (c) however, A and B are independent but become conditionally dependent given C.

Definition 1. ***d-separation*** *(Pearl, 2009): Let A,B,C be the three non-intersecting subsets of nodes in a causal graph $\mathcal{G}$. For any path between two nodes, a collider is a node where arrows of the path meet head-to-head. A path from A to B is said to be* blocked *by C if either a non-collider on the path is in C, or there is a collider on the path and neither the collider nor its descendants are in C.*

If all paths from A to B are blocked, then A is d-separated from B by C: $\text{dsep}(A, B, C) \Rightarrow A \perp\!\!\!\perp B|C$.

B.3. Proof of Proposition 1

Proposition 1 relates to the domain generalization setup, as described in Section 3.1, where the causal feature determines y label without any noise. The distribution of the non-causal feature varies across domains. The proof uses

the entropy formulation of distribution-matching methods, as done by Akuzawa et al. (2019).

Proposition 1. *Under the domain generalization setup as above, if $P(X_c|Y)$ remains the same across domains where x_c is the stable feature, then the class-conditional domain-invariant objective for learning representations yields a generalizable classifier such that the learnt representation $\Phi(\mathbf{x})$ is independent of the domain given x_c. Specifically, the entropy $H(d|x_c) = H(d|\Phi, x_c)$.*

Proof. We can write class-conditional invariant models as optimizing two objectives: minimize the error on the training data (ERM objective), and learn a representation $\Phi(\mathbf{x})$ that is independent of domain given the class label (class-conditional invariant).

Let us focus on the second objective, which be interpreted as 2) maximizing the entropy of domain given class label and representation $H(d|y, \Phi(\mathbf{x}))$. Let Φ_2 be the optimal representation for the class-conditional invariant. We can write,

$$\Phi_2 = \arg\max_{\Phi} H(d|y, \Phi(\mathbf{x})) \tag{5}$$

Since $H(d|y, \Phi(\mathbf{x})) \leq H(d|y)$ using the property of entropy, the optimal Φ_2 satisfies,

$$H(d|y, \Phi_2(\mathbf{x})) = H(d|y) \tag{6}$$

Now two cases arise; $x_c \perp\!\!\!\perp D|Y$ or $x_c \not\perp\!\!\!\perp D|Y$. We assume the former. If X_C is independent of domain conditioned on the class label, then

$$H(d|y) = H(d|y, x_c) \tag{7}$$

Here domain d is independent of both x_c and $\Phi_2(\mathbf{x})$, conditional on y. Since causal features x_c cannot be caused by the representation $\Phi_2(\mathbf{x})$, it cannot be a collider (Definition 1) in any graph connecting d, x_c and $\Phi_2(\mathbf{x})$. Therefore, conditioning on it does not remove the independence between d and $\Phi_2(\mathbf{x})|y$ (conditioned on y). Hence, we condition on Eq 6 with x_c and obtain,

$$H(d|y, x_c) = H(d|y, x_c, \Phi_2(\mathbf{x})) \tag{8}$$

Plugging it into the above equations, we obtain

$$H(d|y) = H(d|y, x_c) = H(d|y, x_c, \Phi_2(\mathbf{x})) \tag{9}$$

Also since there is no label noise, x_c can achieve zero error for predicting the label y. That is, x_c contains all information about y, and thus we can remove y from the above equation,

$$H(d|x_c) = H(d|\Phi_2(\mathbf{x}), x_c) \tag{10}$$

This implies that the learnt representation $\Phi_2(\mathbf{x})$ is independent of the domain given x_c; thus $\Phi_2(\mathbf{x})$ depends on x_c and not on any other feature that changes with domain. □

B.3.1. Remarks based on Proposition 1

If x_c is not independent of domain given class label. However, if X_C is not independent of domain given the class label (i.e., $P(x_c|y)$ changes across domains), then $H(d|y) > H(d|y, x_c)$. Using the equality from Eq 8, we obtain,

$$\begin{aligned} H(d|y) = H(d|y, \Phi_2(\mathbf{x})) &> H(d|y, x_c) \\ H(d|y, \Phi_2(\mathbf{x})) &\geq H(d|\Phi_2(\mathbf{x}), y, x_c) \end{aligned} \tag{11}$$

After removing y as in Eq. 10, $H(d|x_c)$ and $H(d|\Phi_2, x_c)$ may not be equal. In particular, the ground-truth representation $\Phi_{GT}(\mathbf{x}) = x_c$ does not satisfy the class-conditional invariant: $H(d|y, \Phi_{GT}(\mathbf{x})) = H(d|y, x_c) \neq H(d|y)$.

Hence, to learn x_c as the representation, we need a separate constraint, $H(d|x_c) = H(d|\Phi, x_c)$; i.e. domain and representation should be independent conditioned on x_c.

Implications for the slab dataset (Section 3.2). In the slab dataset, $x_c = x_2$ and x_2 is independent of the domain given the class label ($X_2 \perp\!\!\!\perp D|Y$). We also see that $\Phi(\mathbf{x}) = x_2$ satisfies the class-conditional invariant: $H(d|y, x_2) = H(d|y)$ since $X_2 \perp\!\!\!\perp D|Y$. By Proposition 1, the class-conditional invariant should lead to a representation that satisfies $H(d|x_c) = H(d|\Phi(\mathbf{x}), x_c)$. However, the same constraint can also be achieved by setting $\Phi(\mathbf{x}) = x_1$ by shifting the distribution of x_1 slightly. And since there is a simple, linear correlation between x_1 and the class label y, empirically class-conditional methods end up learning a representation dependent on x_1.

B.4. Proof of Proposition 2

Proposition 2. *Given observed data distribution $P(Y, X, D, O)$ that may also include data obtained from interventions on domain D, multiple values of X_C yield exactly the same observational and interventional distributions and hence X_c is unidentifiable.*

Proof. To prove non-identifiability, it is sufficient to show a counter-example where the same structural equations (and hence same observed and interventional distributions over Y, X, D, O) correspond to two different values of X_C.

From Section 4.1, the SCM leads to the following structural equations,

$$\begin{aligned} o &:= g_o(y_{true}, \epsilon_o, \epsilon_{od}) & \mathbf{x}_c &:= g_{xc}(o) \\ \mathbf{x}_a &:= g_{xa}(d, o, \epsilon_{xa}) & \mathbf{x} &:= g_x(\mathbf{x}_c, \mathbf{x}_a, \epsilon_x) \end{aligned} \qquad y := h(\mathbf{x}_c, \epsilon_y)$$

Substituting for $\mathbf{x}_c$ in the SCM equations, we obtain,

$$\begin{aligned} y &= h(g_{xc}(o), \epsilon_y) \\ \mathbf{x} &= g_x(g_{xc}(o), g_{xa}(d, o, \epsilon_{xa}), \epsilon_x) \end{aligned} \tag{12}$$

Given a value of object variable o, note that g_{xc} determines x_c. We now proceed to show that different values of g_{xc} are possible given the same structural equations between the observed variables Y, X, D, O. Specifically, by choosing g_x and h appropriately, different values of g_{xc} can lead to the same observed values for (y, d, o, x).

A simple counter-example. Suppose the following SCM equations,

$$\begin{aligned} y &= h(g_{xc}(o)) \\ x &= g_1(g_{xc}(o)) + g_2(o, d) \end{aligned} \tag{13}$$

Introducing $h^* = h \circ g_{xc}$ and $g_1^* = g_1 \circ g_{xc}$, we can rewrite the above equations as,

$$\begin{aligned} y &= h^*(o) \\ x &= g_1^*(o) + g_2(o, d) \end{aligned} \tag{14}$$

then any g_{xc} is applicable as long as we set h such that $h(g_{xc})(o) = h^*(o)$ and set g_1 such that $g_1(g_{xc}(o)) = g_1^*(o)$. In particular, if the SCM equations are $y = o$, $x = o + o * d$, and we define $h = g_1 = g_{xc}^{-1}$, then g_{xc} can be any invertible function. Hence, different values of $x_c = g_{xc}(o)$ will lead to the same structural equations over Y, X, D, O, and therefore the same observed and interventional distributions. □

B.5. Proof of Theorem 1

Theorem 1. *For a finite number of domains m, as the number of examples in each domain $n_d \to \infty$,*
1. The set of representations that satisfy the condition $\sum_{\Omega(j,k)=1; d \neq d'} \text{dist}(\Phi(\mathbf{x}_j^{(d)}), \Phi(\mathbf{x}_k^{(d')})) = 0$ contains the optimal $\Phi(\mathbf{x}) = X_C$ that minimizes the domain generalization loss in (1).
2. Assuming that $P(X_a|O, D) < 1$ for every high-level feature X_a that is directly caused by domain, and for P-admissible loss functions (Miller et al., 1993) whose minimization is conditional expectation (e.g., ℓ_2 or cross-entropy), a loss-minimizing classifier for the following loss is the true function f^*, for some value of λ.

$$\begin{aligned} f_{\texttt{perfectmatch}} = \arg\min_{h,\Phi} \textstyle\sum_{d=1}^{m} L_d(h(\Phi(X)), Y) + \\ \lambda \textstyle\sum_{\Omega(j,k)=1; d \neq d'} \text{dist}(\Phi(\mathbf{x}_j^{(d)}), \Phi(\mathbf{x}_k^{(d')})) \end{aligned} \tag{3}$$

Proof. **CLAIM 1.** The matching condition can be written as:

$$C(\Phi) = \min_{\Phi} \sum_{d, d' \in D_m} \lim_{\substack{n_d \to \infty \\ n_{d'} \to \infty}} \sum_{\Omega(j,k)=1; d \neq d'} \text{dist}(\Phi(\mathbf{x}_j^{(d)}), \Phi(\mathbf{x}_k^{(d')})) \tag{15}$$

where $\Omega(j, k) = 1$ for pairs of inputs $\mathbf{x}_j$ and $\mathbf{x}_k$ from two different domains d and d' that correspond to the same object. The distance metric dist is non-negative, so the optimal Φ is when $C(\Phi)$ is zero. As in the SCM from Figure 2(b), let X_c represent a feature vector such that it is generated based only on the object O and that it leads to the optimal classifier in (1). From Sections 4.1 and 4.2, we know that $X_c \perp\!\!\!\perp D|O$ and that $x_c = g_{xc}(o)$. Thus, x_c is the same for inputs from the same object and we can write:

$$\text{dist}(\mathbf{x}_{c,j}^{(d)}, \mathbf{x}_{c,k}^{(d')}) = 0 \quad \forall d, d' \in D_m \text{ such that } \Omega(j, k) = 1 \tag{16}$$

Hence, $\Phi(\mathbf{x}) = \mathbf{x}_c$ leads to zero regularizer term and is one of the optimal minimizers for $C(\Phi)$.

CLAIM 2. Further, we show that any other optimal Φ is either a function of $\mathbf{x}_c$ or a constant for all inputs. We prove by contradiction.

Let X_A represent the set of unobserved high-level features that are generated based on both the object O and the domain D. From the SCM from Figure 2(b), a feature vector $X_a \subseteq X_A$ is independent of X_c given the object, $X_a \perp\!\!\!\perp X_c|O$, and $x_a = g_{xa}(d, o, \epsilon_{xa})$. Further, let there be an optimal $\Phi_a(\mathbf{x})$ for $C(\Phi)$ such that it depends on some $X_a \subseteq X_A$ (and is not trivially a constant function). Since Φ_a is optimal, $\Phi_a(\mathbf{x}_j^{(d)}) = \Phi_a(\mathbf{x}_k^{(d')})$ for all d, d' such that $\Omega(j, k) = 1$, where inputs $\mathbf{x}_j$ and $\mathbf{x}_k$ correspond to the same object.

Let us assume that there exists at least one object o for which the effect of domain is stochastic. That is, due to domain-dependent variation, $P(X_a = x_a|D = d, O = o) < 1$. for some d and o. Now consider a pair of inputs $\mathbf{x}_l^{(d)}$ and $\mathbf{x}_i^{(d')}$ from the same object o such that $\Omega(l, i) = 1$, and their corresponding representations are $\Phi_a(\mathbf{x}_l^{(d)})$ and $\Phi_a(\mathbf{x}_i^{(d')})$. Due to domain-dependent variation, with non-zero probability, the high-level X_a features are not the same for these two input data points, $x_{a,l}^{(d)} \neq x_{a,i}^{(d')}$. Since Φ is a deterministic function of $\mathbf{x}$ that is not independent of X_a, if an input $\mathbf{x}$ has a different X_a, its value of $\Phi(\mathbf{x})$ will also be different. Thus, with non-zero probability, we obtain that $\Phi(\mathbf{x}_l^{(d)}) \neq \Phi(\mathbf{x}_i^{(d')})$, unless the effect of X_a is a constant function. Hence, a contradiction and optimal Φ cannot depend on any $X_a \subseteq X_A$ that are generated based on the domain.

Therefore, an optimal solution to $C(\Phi)$ can only depend on X_c. However, any function of X_c is optimal, including trivial functions like the constant function (that will have low accuracy). Below we show that using the ERM term in (3) ensures that the optimal solution contains only those functions of X_C that also maximize accuracy.

Using (2), the empirical optimizer function can be written as (where we scale the loss by a constant $n = \sum_d n_d$, the

total number of training data points):

$$\hat{f}_{pmatch} = \arg\min_{h,\Phi} \frac{1}{n} \sum_{d=1}^{m} \lim_{n_d \to \infty} L_d(h(\Phi(X)), Y) \quad (17)$$

$$\texttt{s.t.} \sum_{\Omega(j,k)=1; d \neq d'} \text{dist}(\Phi(\mathbf{x}_j^{(d)}), \Phi(\mathbf{x}_k^{(d')})) = 0 \quad (18)$$

$$= \arg\min_{h,\psi} \frac{1}{n} \sum_{d=1}^{m} \lim_{n_d \to \infty} L_d(h(\psi(X_c)), Y)$$

$$= \arg\min_{f} \frac{1}{n} \sum_{d=1}^{m} \lim_{n_d \to \infty} L_d(f(X_c), Y) \quad (19)$$

where $\psi(X_c)$ denotes all functions of X_c that are optimal for (15), and the last equality is because $h \circ \psi$ can be written as $f = h \circ \psi$. Since we assume that L is a P-admissible loss function, its minimizer is the conditional expected value. Thus, for any domain d, $\arg\min_f \lim_{n_d \to \infty} \frac{1}{n_d} L_d(f(X_c), Y) = \mathbb{E}[Y|X_c, D]$. Further, by d-separation, $Y \perp\!\!\!\perp D | X_c$. Therefore, $\mathbb{E}[Y|X_c, D] = \mathbb{E}[Y|X_c]$. The above equation indicates that the loss minimizer function on any domain is independent of the domain. Thus, for the m training domains, we can write:

$$\arg\min_{f \in \mathcal{F}} \lim_{n_d \to \infty} \frac{1}{n_d} L_d(f(X_c), Y) = \arg\min_{f \in \mathcal{F}} \mathbb{E}[l(f(\mathbf{x}_c), y)]$$
$$= \mathbb{E}[Y|X_c] \quad \forall d \in D_m \quad (20)$$

Now (19) can be rewritten as,

$$\hat{f}_{pmatch} = \arg\min_{f} \frac{1}{n} \sum_{d=1}^{m} \lim_{n_d \to \infty} \frac{L_d(f(X_c), Y)}{n_d} n_d$$
$$= \arg\min_{f} \sum_{d=1}^{m} \lim_{n_d \to \infty} \frac{L_d(f(X_c), Y)}{n_d} \frac{n_d}{n} \quad (21)$$

From the equation above, the loss for $\hat{f}_{pmatch}$ can be considered as a weighted sum of the average loss on each training domain where the weights are all positive. Since $E[Y|X_c]$ minimizes the average loss on each domain as $n_d \to \infty$, it will also minimize the overall weighted loss for all values of the weights. Therefore, for any dataset over m domains in D_m, $\mathbb{E}[Y|X_c]$ is the optimal function that minimizes the overall loss.

Moreover, we can also write f^* as:

$$f^* = \arg\min_{f \in \mathcal{F}} \mathbb{E}_{(d,\mathbf{x},y)}[l(y, f(\mathbf{x}))]$$
$$= \arg\min_{h \in \mathcal{F}} \mathbb{E}_{(d,\mathbf{x},y)}[l(y, h(\mathbf{x}_c))] \quad (22)$$
$$= \arg\min_{h \in \mathcal{F}} \mathbb{E}_{(\mathbf{x},y)}[l(y, h(\mathbf{x}_c)] = \mathbb{E}[Y|X_c]$$

where we utilize (20) and that the loss function is P-admissible. Hence, $f^* = \mathbb{E}[Y|X_c]$ is the loss-miniziming function for the loss in (19).

Finally, using a Lagrangian multiplier, minimizing the following soft constraint loss is equivalent to minimizing (18), for some value of λ.

$$\hat{f}_{\texttt{pmatch}} = \lim_{\forall d \in D_m n_d \to \infty} \arg\min_{h,\Phi} \sum_{d=1}^{m} L_d(h(\Phi(X)), Y)$$
$$+ \lambda \sum_{\Omega(j,k)=1; d \neq d'} \text{dist}(\Phi(\mathbf{x}_j^{(d)}), \Phi(\mathbf{x}_k^{(d')})) \quad (23)$$

The result follows. □

Comment on Theorem 1. In the case where the effect of a domain is also deterministic, it is possible that $P(X_a|O, D) = 1$ (e.g., in artificially created domains like Rotated-MNIST where every object is rotated by the *exact* same amount in each domain). In that case Theorem 1 does not apply and it is possible to learn a representation Φ_a that depends on $X_a \subseteq X_A$ and still minimizes $C(\Phi)$ to attain $C(\Phi) = 0$. For example, with two training domains on Rotated-MNIST dataset ($0°$, $\alpha°$), it is possible to learn a representation that simply memorizes to "un-rotate " the α angle back to $0°$. Such a representation will fail to generalize to domains with different rotation angles, but nonetheless minimizes $C(\Phi)$ by attaining the exact same representation for each object.

In practice, we conjecture that such undesirable Φ_a are avoided by model-size regularization during training. As the number of domains increase, it may be simpler to learn a single transformation (representation) based on X_c (and independent of X_c features like angle) than learn separate angle-wise transformations for each train domain.

B.6. Proof of Proposition 3

Domain-invariant representations. ($\Phi(\mathbf{x}) \perp\!\!\!\perp D$) (Muandet et al., 2013; Li et al., 2018b; Ganin et al., 2016). Using d-separation on the SCM from Figure 2(b), $X_C \perp\!\!\!\perp D$ is not sufficient since O blocks the path between X_C and D. While (Zhao et al., 2019) argue that this condition fails when Y is correlated with D, our analysis shows that domain-invariant methods require a stronger condition that both class label and actual objects sampled be independent of domain.

Class-conditional domain-invariant. ($\Phi(\mathbf{x}) \perp\!\!\!\perp D|Y$.) (Li et al., 2018c; Ghifary et al., 2016; Li et al., 2018d) Even in the ideal case where we observe Y_{true}, d-separation on the SCM reveals that $X_C \not\perp\!\!\!\perp D|Y_{true}$ due to a path through O. Thus, having the same distribution per class is not consistent with properties of X_C.

Below we prove these results formally.

Proposition 3. *The conditions enforced by domain-invariant ($\Phi(x) \perp\!\!\!\perp D$) or class-conditional domain-invariant ($\Phi(x) \perp\!\!\!\perp D|Y$) methods are not satisfied by the causal representation X_C. Thus, without additional assumptions, the set of representations that satisfy any of these conditions does not contain X_C, even as $n \to \infty$.*

Proof. As in the SCM from Figure 2(b), let X_c represent an unobserved high-level feature vector such that it is generated based only on the object O and that it leads to the optimal classifier in (1). From Sections 4.1 and 4.2, we know that $X_c \perp\!\!\!\perp D|O$ and that $x_c = g_{xc}(o)$. Following a similar proof to Theorem 1 (Claim 1), we check whether $\Phi(\mathbf{x}) = \mathbf{x}_c$ satisfies the invariance conditions required by the two methods.

1. **Domain-invariant**: The required condition for a representation is that $\Phi_{\texttt{DI}}(\mathbf{x}) \perp\!\!\!\perp D$. But using the d-separation criteria on the SCM in Figure 2(b), we find that $X_c \not\perp\!\!\!\perp D$ due to a path through Object O.

2. **Class-conditional domain-invariant**: The required condition for a representation is that $\Phi_{\texttt{CDI}} \perp\!\!\!\perp D|Y$. However using the d-separation criteria on the SCM, we find that $X_c \not\perp\!\!\!\perp D|Y$ due to a path through Object O that is not blocked by Y (nor by Y_{true} if it is observed).

Therefore, under the conditions proposed by these methods, X_c or any function of X_c is not an optimal solution without making any additional assumptions. Hence, even with infinite samples, a method optimizing for these conditions will not retrieve X_c. □

C. Evaluation and implementation details

In this section we describe implementation details for our proposed methods. We also discuss the evaluation protocol, including details about hyperparameters and cross-validation.

C.1. Implementation details

For the implementation of `ERM-PerfMatch` in Eq. (3); we use the cross-entropy loss for L_d and l_2 distance for dist in Eq. (3). Similarly, we implement the `ERM-RandMatch` with a match function Ω in Eq. (3) that randomly matches data points across domains with the same class, For both methods, we consider the representation $\Phi(\mathbf{x})$ to be the last layer of the network. That is, we take h to be identity function in Eq. (3) for simplicity. It is also possible to use the second-last or any other previous layer as a representation, but the last layer performed well in our experiments. Also, given a fixed data point, the match function Ω could select multiple data points as potential matches for it. In this case we use Eq. (3) with stochastic matching, where we randomly select one match out of the potential multiple matches.

We use SGD to optimize the loss for all the datasets, with details about learning rate, epochs, batch size, weight decay etc. provided in the section C.3 ahead. For all the different methods, we sample batches from the data matrix consisting of data points matched across domains; hence we ensure an equal number of data points from each source domain in a batch. When training with `MatchDG`, the underlying architecture for Phase 2 is kept the same for ERM, `RandMatch`, `PerfMatch` for the respective task; with the details mentioned below for each dataset. The details for the Phase-1 architecture are specified in section C.3, Table 9.

Rotated MNIST & Fashion-MNIST. The datasets contain rotations of grayscale MNIST handwritten digits and fashion article images from $0°$ to $90°$ with an interval of $15°$ (Ghifary et al., 2015), where each rotation angle represents a domain and the task is to predict the class label. For Table 2, we follow the setup in CSD (Piratla et al., 2020), we report accuracy on $0°$ and $90°$ together as the test domain and the rest as the train domains. We use $2,000$ and $10,000$ training samples from each domain for rotated MNIST and Fashion-MNIST, and train models using Resnet-18 architecture (without pre training). We choose this as our primary setup and select $0°$ and $90°$ as our target domain, since these are known to be the most difficult domains to generalize (Piratla et al., 2020; Motiian et al., 2017).

Further, we also evaluate on other setups of Rotated MNIST in prior works (Motiian et al., 2017; Gulrajani & Lopez-Paz, 2020), which involve six domains ($0°$, $15°$, $30°$, $45°$, $60°$, $75°$), and evaluate for each domain being the target domains with the remaining five used as source domains. We sample 1000 data points for each domain and evaluate using the LeNet architecture (Table 11) as per the setup proposed by (Motiian et al., 2017). Similarly, we sample all the 70,000 images in MNIST and evaluate using the custom architecture (Table 12) as per the setup proposed by (Gulrajani & Lopez-Paz, 2020).

Another important distinction between different setups above is the use of different digits for the source and the target domains ((Piratla et al., 2020), (Gulrajani & Lopez-Paz, 2020)), as opposed to the use of same digits across the source and the target domains in setup of (Motiian et al., 2017) which makes the task easier as it leaks information about the target domains.

Finally, for all the different setups proposed above, we create an additional validation set for each domain with

20% percent size as of the training set for that domain. We use the validation set from the source domains for hyper parameter tuning.

PACS. This dataset contains total 9991 images from four domains: Photos (P), Art painting (A), Cartoon (C) and Sketch (S). The task is to classify objects over 7 classes. Following (Dou et al., 2019), we train 4 models with each domain as the target using Resnet-18 (Table 4), Resnet-50 (Table 5) and Alexnet (Table 18), with each architecture pre-trained on ImageNet. We also the following data augmentations (Gulrajani & Lopez-Paz, 2020) while training: Random Crop, Horizontal Flip, Color Jitter, and Random Gray Scale.

Chest X-ray. We use Chest X-rays images from three different sources: NIH (Wang et al., 2017), ChexPert (Irvin et al., 2019) and RSNA (rsn, 2018). The task is to detect whether the image corresponds to a patient with Pneumonia (1) or not (0). For ease of interpretation, we balance the data such that there are equal number of images per class in each domain. Since majority of the images in each domain correspond to the class (0), we sample a subset of the images to ensure that there is no class imbalance in each domain. The dataset size for the different splits on each domain are described below:

- NIH: Train (800), Validation (200), Test (400)
- ChexPert: Train (800), Validation (200), Test (400)
- RSNA: Train (800), Validation (200), Test (400)

Following prior works (Cohen et al., 2020), we use the pre-trained DenseNet-121 architecture for classification. We use the following data augmentations: Random Crop and Random Horizontal Flip. We further create spurious correlations, all the images of the class 0 in the training domains are translated vertically downwards; while no such translation is done for the test domain. We translate the images in each source domain by a fixed amount, which varies over different source domains (NIH (45), ChexPert (35), RSNA (15)). This leads to a downward shift in the position of lungs in the images for the class 0 as compared to those for class 1, which could lead to models utilizing this spurious relative difference in position of lungs for the classifications task.

C.1.1. MatchDG implementation details:

The MatchDG algorithm proceeds in two phases.
Initialization: We construct matches of pairs of same-class data points from different domains. Hence, given each data point we randomly select another data point with the same class from another domain. The matching for each class across domains is done relative to a base domain; which is chosen by taking the domain that has the highest number of samples for that class. This is done to avoid missing out on data points when there is class imbalance across domains. Specifically, we iterate over classes and for each class, we match data points randomly across domains w.r.t a base domain for that class. This leads to matrix $\mathcal{M}$ of size $(N^{'}, K)$, where $N^{'}$ refers to the updated domain size (sum of the size of base domain for all the classes) and K refers to the total number of domains. We describe the two phases below:

Phase 1: We samples batches (B, K) from the matched data matrix $\mathcal{M}$, where B is the batch size. For each data point x_i in the batch, we minimize the contrastive loss from (4) by selecting its matched data points across domains as the positive matches and consider every data point with a different class label from x_i to be a negative match.

After every t epochs, we periodically update the matched data matrix by using the representations learnt by contrastive loss minimization. We follow the same procedure of selecting a base domain for each class, but instead of randomly matching data points across domains, we find the nearest neighbour for the data point in base domain among the data points in the other domains with the same class label based on the l_2 distance between their representations.

At the end of Phase I, we update the matched data matrix based on l_2 distance over the final representations learnt. We call these matches as the *inferred* matches.

Phase 2: We train using the loss from Eq. (3), with the match function Ω based on the inferred matches generated from Phase 1 (ERM + Inferred Match). We train the network from scratch in Phase 2 and use the representations learnt in Phase 1 to only update the matched data matrix.

The updated data matrix based on representations learnt in Phase 1 may lead to many-to-one matches from the base domain to the other domains. This can lead to certain data points being excluded from the training batches. Therefore, we construct batches such that each batch consists of two parts. The first is sampled as in Phase 1 from the matched data matrix. The second part is sampled randomly from all train domains. Specifically, for each batch (B, K) sampled from the matched data matrix, we sample an additional part of size B with data points selected randomly across domains. The loss for the second part of the batch is simply ERM, along with ERM + InferredMatch Loss on the first part of the batch.

C.2. Metrics for evaluating quality of learnt matches

Here we describe the three metrics used for measuring overlap of the learnt matches with ground-truth "perfect"

Table 8. Hyper parameter selection details for all the datasets. We mention the Optimal Value for each hyper parameter and the Range used for grid search. We leave the optimal value for Epochs as blank since we do early stopping based on validation loss, with the total number of epochs for model training specified in the Range column. For the dataset PACS, since the optimal values differ for different test domains, we represent them separately in Table 10

Dataset	Hyper Parameter	Optimal Value	Range
Rotated & Fashion MNIST Table 2 (ResNet-18)	Total Epochs	-	25
	Learning Rate	0.01	[0.01]
	Batch Size	16	[16]
	Weight Decay	0.0005	[0.0005]
	Match Penalty	0.1	[0.1, 1.0]
	IRM Penalty	1.0 (RotMNIST); 0.05 (FashionMNIST)	[0.05, 0.1, 0.5, 1.0, 5.0]
	IRM Threshold	5 (RotMNIST), 0 (FashionMNIST)	[0, 5, 15, 20]
Rotated MNIST Table 11 (LeNet)	Total Epochs	-	100
	Learning Rate	0.01	[0.01]
	Batch Size	16	[16]
	Weight Decay	0.0005	[0.0005]
	Match Penalty	1.0	[0.1, 1.0]
Rotated MNIST Table 12 (DomainBed)	Total Epochs	-	25
	Learning Rate	0.01	[0.01]
	Batch Size	128	[16, 32, 64, 128]
	Weight Decay	0.0005	[0.0005]
	Match Penalty	1.0	[0.1, 1.0]
PACS Table 17, 18 (ResNet-18, ResNet-50, AlexNet)	Total Epochs	-	50
	Learning Rate	Table 10	[0.01, 0.001, 0.0005]
	Batch Size	16	[16]
	Weight Decay	0.0005	[0.0005]
	Match Penalty	Table 10	[0.01, 0.1, 0.5, 1.0, 5.0]
Chest X-ray Table 6 (DenseNet-121)	Total Epochs	-	40
	Learning Rate	0.001	[0.01, 0.001]
	Batch Size	16	[16]
	Weight Decay	0.0005	[0.0005]
	Match Penalty	10.0 (`RandMatch`), 50.0 (`MatchDG`, `MDGHybrid`)	[0.1, 1.0, 10.0, 50.0]
	IRM Penalty	10.0	[0.1, 1.0, 10.0, 50.0]
	IRM Threshold	5	[0, 5, 15, 20]

matches.

`Overlap %`: Percentage of matches (j, k) as per the perfect match strategy Ω that are also consistent with the learnt match strategy $\Omega^{'}$.

$$\frac{\sum_{\Omega(j,k)=1;d\neq d'} \Omega^{'}(j,k)}{\sum_{\Omega(j,k)=1;d\neq d'} 1} \tag{24}$$

`Top-10 Overlap %`: Percentage of matches (j, k) as per the perfect match strategy Ω that are among the Top-10 matches for the data point j w.r.t the learnt match strategy $\Omega^{'}$ i.e. $S^{10}_{\Omega'}(j)$

$$\frac{\sum_{\Omega(j,k)=1;d\neq d'} \mathbb{1}[k \in S^{10}_{\Omega'}(j)]}{\sum_{\Omega(j,k)=1;d\neq d'} 1} \tag{25}$$

`Mean Rank`: For the matches (j, k) as per the perfect match strategy Ω, compute the mean rank for the data point j w.r.t the learnt match strategy $\Omega^{'}$ i.e. $S_{\Omega'}(j)$

$$\frac{\sum_{\Omega(j,k)=1;d\neq d'} Rank[k \in S_{\Omega'}(j)]}{\sum_{\Omega(j,k)=1;d\neq d'} 1} \tag{26}$$

C.3. HyperParameter Tuning

To select hyperparameters, prior works (Dou et al., 2019; Carlucci et al., 2019; Li et al., 2018a) use leave-one-domain-out validation, which means that the hyperparameters are tuned after looking at data from the unseen domain. Such a setup is violates the premise of the domain generalization task that assumes that a model should have no access to the test domain. Therefore, in this work, we construct a validation set using only the source domains and use it for hyper parameter tuning. In the case of PACS, we already have access to the validation indices for each domain and use them to construct a validation set based on the source domains. For Rotated & Fashion MINST, Chest X-ray datasets, we create validation set for each source domain as described in the section B.1 above. Hence, the model does not have

Table 9. `MatchDG` Phase 1 training details for all the datasets.We did not do hyper parameter tuning as we did for other methods, hence we mention the default value for each hyper parameter that we used. Please note we still did early stopping, the Total Epochs in the table reflects the max budget for training. The specific archiecture used for Phase 1 training is also mentioned for each dataset.

Dataset	Hyper Parameter	Default Value
Rotated & Fashion MNIST Table 2, 11, 12	Total Epochs	50
	Learning Rate	0.01
	Batch Size	64 (Table 2), 512 (Table 11, Table 12)
	Weight Decay	0.0005
	τ	0.05
	Architecture	ResNet-18 (Table 2), LeNet (Table 11), Custom CNN (Table 12)
PACS Table 17, 18	Total Epochs	50
	Learning Rate	0.01
	Batch Size	32
	Weight Decay	0.0005
	τ	0.05
	Architecture	ResNet-50
Chest X-ray Table 6	Total Epochs	50
	Learning Rate	0.01
	Batch Size	32
	Weight Decay	0.0005
	τ	0.05
	Architecture	DenseNet-121

access to the data points from the target/test domains at the time of training and validation.

We perform a grid search over pre-defined values for each hyper parameter and report the optimal values along with the values used for grid search in Table 8. Further, we do early stopping based on the validation accuracy on source domains and use the models which obtain the best validation accuracy.

For the case of `MatchDG` Phase-1, we do not perform grid search and use default values for each hyper parameter (Table 9). We still do early stopping for `MatchDG` Phase-1, based on the metric `Top-10 Overlap` (Section B.2) over the validation set of source domains. Since we require perfect matches for the evaluation of the metric `Top-10 Overlap`, we create prefect matches using the self augmentations (Section B.1) for each dataset.

C.4. Reproducing Results from Prior Work

MNIST and Fashion MNIST The results for MASF, CSD, and IRM in Table 2 were computed using their code which is available online [1][2][3]. The MASF code was hard-coded to run for PACS dataset; which has 3 source domains that gets divided into 2 meta train and 1 meta test domain. Their code requires atleast 2 meta train domains; which leads to an issue for only 2 source domains (30, 45). In Table 2 when there are only 2 source domains; their code considers only 1 meta train domain. To resolve this issue; we create a copy of the 1 meta train domain and thus run MASF for source domains 30, 45 on MNIST.

The results for prior approaches in Table 11 are taken from (Shankar et al., 2018), (Ilse et al., 2020). For the results using DomainBed setup in Table 12, the results for prior approaches are taken from (Gulrajani & Lopez-Paz, 2020).

PACS We did not generate results for the prior approaches for PACS by developing or using existing implementations. All the results for the prior approaches on PACS were taken from the respective papers as specified in the Table 17, 18.

Chest X-ray The results for the prior approaches CSD, IRM were generated using the implementations of both of the methods available on github [1,3] .

D. Additional Evaluation on Rotated MNIST and Fashion-MNIST

Here we present results for additional experiments on Rotated MNIST and Fashion-MNIST datasets using `MatchDG`.

D.1. Comparing `MatchDG` with prior work on the LeNet Network

Table 11 compares the accuracy results for `MatchDG` with prior work on the LeNet architecture (Motiian et al., 2017). In this setup, there are six domains in total

[1]https://github.com/vihari/CSD
[2]https://github.com/biomedia-mira/masf
[3]https://github.com/facebookresearch/InvariantRiskMinimization

Table 10. Optimal values for hyper parameters on PACS. Batch Size (16), Weight Decay (0.0005) was consistent across different cases. The Match Penalty for the method `MDGHybrid` corresponds to (`MatchDG` penalty, `PerfMatch` penalty).

Architecture	Hyper Parameter	Test Domain	ERM	`RandMatch`	`MatchDG`(Phase 2)	`MDGHybrid`
ResNet-18 Table 4, 17	Learning Rate	Photo	0.001	0.001	0.0005	0.0005
		Art Painting	0.01	0.01	0.001	0.001
		Cartoon	0.01	0.001	0.001	0.001
		Sketch	0.01	0.01	0.01	0.01
	Match Penalty	Photo	0	5.0	1.0	(0.1, 0.1)
		Art Painting	0	0.1	5.0	(0.01, 0.1)
		Cartoon	0	5.0	1.0	(0.1, 0.1)
		Sketch	0	0.5	0.5	(0.01, 0.1)
ResNet-50 Table 5, 17	Learning Rate	Photo	0.0005	0.0005	0.0005	0.0005
		Art Painting	0.01	0.01	0.001	0.001
		Cartoon	0.01	0.01	0.001	0.0005
		Sketch	0.01	0.01	0.0005	0.001
	Match Penalty	Photo	0	5.0	0.01	(0.1, 0.1)
		Art Painting	0	0.1	0.1	(0.01, 0.1)
		Cartoon	0	0.01	0.01	(0.01, 0.1)
		Sketch	0	0.1	5.0	(0.01, 0.1)
AlexNet Table 18	Learning Rate	Photo	0.0005	0.0005	0.0005	0.0005
		Art Painting	0.001	0.001	0.001	0.001
		Cartoon	0.001	0.001	0.001	0.001
		Sketch	0.0005	0.001	0.001	0.001
	Match Penalty	Photo	0	0.1	0.1	(0.1, 0.1)
		Art Painting	0	0.1	1.0	(0.01, 0.1)
		Cartoon	0	0.5	1.0	(0.01, 0.1)
		Sketch	0	0.5	0.1	(0.01, 0.1)

$(0°, 15°, 30°, 45°, 60°, 75°)$. For each test domain, the remaining five domains are used as source training domains. We observe that matching-based training methods `RandMatch` and `MatchDG` outperform prior work on the all the domains except the test domain 0, where `MatchDG` is competitive to the best performing approach DIVA. They also achieve accuracy almost equal to the oracle case `PerfMatch` for target angles ($15°$ to $60°$) that lie in between the source domains.

D.2. Comparing `MatchDG` on Domain Bed Benchmark

Table 12 compares the accuracy results for `MatchDG` with prior work on the setup proposed by (Gulrajani & Lopez-Paz, 2020). This setup is similar to the setup in the section D.1, however, it uses a custom CNN architecture and all the $70,000$ images for each domain. For a fair comparison, we use the same custom CNN architecture for learning the match function during the `MatchDG` Phase-I. Even under this constraint, `MatchDG` average accuracy is only 0.5% percent behind the best performing approaches (CORAL, MMD). As supported by our experiments before (Table 2, 3) we believe that using more powerful architectures (ResNet-18, ResNet-50) during the `MatchDG` Phase-1 should help in learning a better match function and consequently better average accuracy.

D.3. Accuracy Results using a fraction of perfect matches

To show the importance of learning a good match function, we present the results of approaches with match function capturing some fixed percentage of perfect matches in the Table 13. For both Rotated & Fashion MNIST, we observe that the approaches that contain a higher proportion of perfect matches perform better in terms of accuracy on target domains. Hence, the quality of the match function leads to monotonic effect on the generalization performance of the matching approaches.

D.4. Quality of representation learnt in the classification phase

In addition to Table 3 that shows metrics for Phase 1 of `MatchDG`, we compute the metrics for the classification phase (Phase 2) of `MatchDG`. Specifically, we compute the Overlap, Top-10 overlap and the Mean Rank metrics (Section C.2) for matched pairs of inputs based on the representation learnt at the end of the classification phase.

Table 14 shows the matching metrics for `MatchDG` and compares it to the matches based on the representations (last layers) learnt by the `ERM-PerfMatch` and `ERM-RandMatch` methods. For both Rotated-

Table 11. Accuracy for Rotated MNIST datasets using the LeNet architecture as proposed in (Motiian et al., 2017). The results for the prior approaches CCSA (Motiian et al., 2017), D-MTAE (Ghifary et al., 2015), LabelGrad (Goodfellow et al., 2014), DAN (Ganin et al., 2016), and CrossGrad (Shankar et al., 2018) are taken from Table 9 in (Shankar et al., 2018). The results for DIVA (Ilse et al., 2020) are taken from the Table 1 in their paper.

Algorithm	0	15	30	45	60	75	Average
ERM	88.2 (1.0)	98.6 (0.5)	97.7 (0.6)	97.5 (0.3)	97.0 (0.1)	85.6 (2.1)	94.1
CCSA	84.6	95.6	94.6	82.9	94.8	82.1	89.1
D-MTAE	82.5	96.3	93.4	78.6	94.2	80.5	87.6
LabelGrad	89.7	97.8	98.0	97.1	96.6	92.1	95.2
DAN	86.7	98.0	97.8	97.4	96.9	89.1	94.3
CrossGrad	88.3	98.6	98.0	97.7	97.7	91.4	95.3
DIVA	**93.5** (0.3)	99.3 (0.1)	99.1 (0.1)	99.2 (0.1)	99.3 (0.1)	93.0 (0.4)	97.2
`RandMatch`	91.0 (0.9)	**99.7** (0.2)	99.6 (0.1)	**99.4** (0.1)	**99.7** (0.1)	93.1 (1.1)	97.1
`MatchDG`	93.0 (0.5)	99.5 (0.3)	**99.9** (0.1)	**99.4** (0.1)	**99.7** (0.3)	**93.3** (1.1)	**97.4**
`PerfMatch`	96.5 (0.6)	99.1 (0.3)	99.2 (0.3)	98.6 (0.7)	98.6 (1.0)	94.9 (1.8)	97.8

Table 12. Accuracy for Rotated MNIST datasets using the DomainBed setup as proposed in (Gulrajani & Lopez-Paz, 2020). The results for the approaches IRM (Arjovsky et al., 2019), DRO (Sagawa et al., 2019), Mixup (Xu et al., 2019; Yan et al., 2020; Wang et al., 2020), MLDG (Li et al., 2018a), CORAL (Sun & Saenko, 2016), MMD (Li et al., 2018b), DANN (Ganin et al., 2016), C-DANN (Li et al., 2018d) are taken from (Gulrajani & Lopez-Paz, 2020).

Algorithm	0	15	30	45	60	75	Average
ERM	95.6 (0.1)	99.0 (0.1)	98.9 (0.0)	99.1 (0.1)	**99.0** (0.0)	**96.7** (0.2)	98.0
IRM	95.9 (0.2)	98.9 (0.0)	99.0 (0.0)	98.8 (0.1)	98.9 (0.1)	95.5 (0.3)	97.9
DRO	95.9 (0.1)	98.9 (0.0)	99.0 (0.1)	99.0 (0.0)	**99.0** (0.0)	96.9 (0.1)	**98.1**
Mixup	96.1 (0.2)	**99.1** (0.0)	98.9 (0.0)	99.0 (0.0)	99.0 (0.1)	96.6 (0.1)	**98.1**
MLDG	95.9 (0.2)	98.9 (0.1)	99.0 (0.0)	**99.1** (0.0)	**99.0** (0.0)	96.0 (0.2)	98.0
CORAL	95.7 (0.2)	99.0 (0.0)	**99.1** (0.1)	**99.1** (0.0)	**99.0** (0.0)	**96.7** (0.2)	**98.1**
MMD	**96.6** (0.1)	98.9 (0.0)	98.9 (0.1)	99.1 (0.1)	**99.0** (0.0)	96.2 (0.1)	**98.1**
DANN	95.6 (0.3)	98.9 (0.0)	98.9 (0.0)	99.0 (0.1)	98.9 (0.0)	95.9 (0.5)	97.9
C-DANN	96.0 (0.5)	98.8 (0.0)	99.0 (0.1)	**99.1** (0.0)	98.9 (0.1)	96.5 (0.3)	98.0
`RandMatch`	95.4 (0.4)	98.2 (0.1)	97.9 (0.5)	98.5 (0.1)	98.1 (0.1)	94.3 (0.3)	97.1
`MatchDG`	95.9 (0.1)	98.4 (0.1)	98.6 (0.2)	98.9 (0.2)	98.7 (0.1)	95.1 (0.3)	97.6

Table 13. Accuracy results using a fraction of perfect matches during training

	MNIST	Fashion-MNIST
RandMatch	93.4 (0.26)	77.0 (0.42)
Approx 25%	93.8 (0.48)	77.8 (0.79)
Approx 50%	94.0 (0.42)	78.0 (0.78)
Approx 75%	94.7 (0.14)	78.9 (0.31)
PerfMatch (100%)	96.0 (0.41)	81.6 (0.46)

MNIST and Fashion-MNIST datasets, `MatchDG` obtains mean rank, Top 10 overlap and total overlap between `ERM-PerfMatch` and `ERM-RandMatch`. As the Fashion-MNIST dataset is more complex than the digits dataset, we observe that the mean rank with different training techniques is higher than the corresponding values for the Rotated-MNIST dataset.

D.5. Matching metrics for Fashion-MNIST dataset with 2000 training samples per domain

In the main text (Table 3), we computed matching metrics for MatchDG (Phase 1) over the Fashion-MNIST dataset with 10000 samples per domain. Here we compute the same metrics for a smaller dataset with 2000 samples per domain.

We compute the metric for the default instantiation of Phase 1 of `MatchDG` initialized with random matches and compare it to an *oracle* version of `MatchDG` initialized with perfect matches. In addition, we compare the metrics for matches generated using baseline ERM (last layer of the network) in order to understand its effectiveness as a matching strategy in Phase 1. Table 15 shows the metrics for Phase 1 of `MatchDG` with 2K images from the Fashion-MNIST dataset, and reproduces the metrics for the 10K dataset from Table 3 for ease of comparison. We observe that the mean rank of perfect matches improves for the smaller dataset. Similarly, the overlap and top-10 overlap also increase for

Table 14. Mean rank, Top-10 overlap, and overlap metrics for the matches learnt in the classification phase (Phase 2), when trained on all five source domains in the Rotated MNIST and FashionMNIST datasets.

Dataset	Method	Overlap (%)	Top 10 Overlap (%)	Mean Rank
Rotated MNIST	RandMatch	2.2 (0.18)	13.5 (0.36)	75.5 (1.65)
	MatchDG (Phase 2)	**17.7** (0.97)	**41.8 (2.89)**	**39.6 (3.58)**
	PerfMatch (Oracle)	78.2 (1.91)	95.5 (1.37)	1.84 (0.67)
Fashion MNIST (10k)	RandMatch	0.5 (0.04)	3.2 (0.17)	420.0 (7.27)
	MatchDG (Phase 2)	**1.8 (0.13)**	**8.5 (0.56)**	**296.5 (9.94)**
	PerfMatch (Oracle)	9.2 (0.21)	30.5 (0.38)	114.7 (3.29)

the smaller dataset. A possible reason is that there are fewer alternative matches to the perfect match as the number of samples is reduced. That said, while the overlap with perfect matches may decrease as sample size increases, the accuracy of the resultant classifier may still increase due to higher sample size.

D.6. Iterative updating of matches in Phase-1 of MatchDG

In Section 5.1, we proposed Phase 1 of the `MatchDG` algorithm with iterative updates to the computed matches. Here we compare the quality of matches learnt at the end of Phase 1 with or without using the iterative updating. Without the iterative updates, the matches always remain the same as the random matches with which the algorithm was initialized.

Table 16 shows metrics computed at the end of Phase 1 of `MatchDG` using both an iterative approach vs. a non-iterative approach. The iterative approach provides a $2\times$ improvement on the overlap with perfect matches for rotated MNIST and Fashion-MNIST datasets. Since higher overlap in the inferred matches results in better classification accuracy in Phase 2 (as shown in Table 13), we conclude that using the iterative approach improves the domain generalization capability of `MatchDG`.

Table 15. Metrics computed at `MatchDG` (Phase 1) for Fashion-MNIST dataset with 2K and 10K sample size used for training. Lower is better for mean rank.

Dataset	Method	Overlap (%)	Top 10 Overlap (%)	Mean Rank
Fashion MNIST (2k)	ERM	8.7 (0.14)	36.0 (1.41)	36.1 (1.66)
	`MatchDG` (Default)	**38.5** (2.11)	**71.2** (0.91)	**15.9** (0.54)
	`MatchDG` (PerfMatch)	69.5 (10.8)	91.9 (5.8)	3.3 (2.4)
Fashion MNIST (10k)	ERM	2.1 (0.12)	11.1 (0.63)	224.3 (8.73)
	`MatchDG` (Default)	**17.9** (0.62)	**43.1** (0.83)	**89.0** (3.15)
	`MatchDG` (PerfMatch)	56.2 (1.79)	87.2 (1.48)	7.3 (1.18)

Table 16. Overlap with perfect matches, top-10 overlap and the mean rank for perfect matches for Iterative and Non Iterative `MatchDG` over all training domains. Lower is better for mean rank.

Dataset	Method (Phase 1)	Overlap (%)	Top 10 Overlap (%)	Mean Rank
MNIST	`MatchDG` (Iterative)	**28.9** (1.24)	**64.2** (2.42)	**18.6** (1.59)
	`MatchDG` (Non Iterative)	12.3 (0.28)	37.9 (0.27)	37.8 (0.47)
Fashion MNIST (10k)	`MatchDG` (Iterative)	**17.9** (0.62)	**43.1** (0.83)	**89.0** (3.15)
	`MatchDG` (Non Iterative)	7.7 (0.28)	23.8 (0.78)	153.9 (9.63)

E. Additional Evaluation on PACS

E.1. ResNet Results

Table 17 extends the evaluation on PACS with ResNet-18, ResNet-50 (Table 4, 5) in the main text by adding comparison with more prior approaches. We observe that `MDGHybrid` beats most of the prior approaches on both the ResNet-18 and ResNet-50 evaluation, except DDEC (Asadi et al., 2019), and RSC (Huang et al., 2020). However, as stated in the main paper, DDEC (Asadi et al., 2019) rely on data from additional source like Behance BAM! dataset and we are also not sure about the validation mechanism used by them. If the validation mechanism used by them includes data from the target domain during validation, then `MatchDG` (Test), `MDGHybrid` (Test) obtain better accuracy than them.

E.2. AlexNet Results

Finally, we compare `RandMatch` and `MatchDG` to prior work on generalization accuracy for the PACS dataset using the AlexNet architecture. As in Table 17, the task is to generalize to a test domain after training on the remaining three domains.

For all test domains, Table 18 shows that both `RandMatch` and `MatchDG` outperform the baseline ERM method. Averaging over the test domains, `MDGHybrid` provides improvement over `MatchDG` (70.46 versus 69.91). Moreover, on average `MatchDG`, `MDGHybrid` are better than many previous approaches D-MTAE (Ghifary et al., 2015), DBADG (Li et al., 2017), CIDDG (Li et al., 2018d), HEX (Wang et al., 2019) and FeatureCritic (Li et al., 2019b), but some other methods like MASF (Dou et al., 2019), DGER (Zhao et al., 2020), RSC (Huang et al., 2020) achieve higher accuracy than `MatchDG`. Since `MatchDG` outperforms most of the prior work on the same dataset when trained using ResNet-18, ResNet-50 architecture (Table 17), we speculate that `MatchDG` requires a powerful underlying network architecture to use matches effectively for classification.

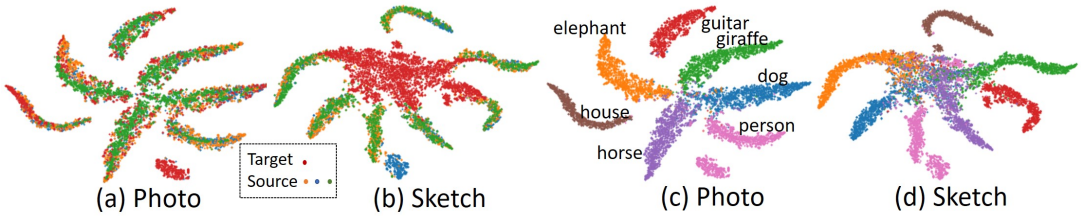

Figure 5. The t-SNE plots for visualizing features learnt in `MatchDG` Phase 1. (a)-(c) are for Photo as the target domain and (b)-(d) are for Sketch.

E.3. T-SNE Plots

Beyond accuracy, we investigate the quality of representations learnt by MatchDG using t-SNE (Maaten & Hinton, 2008) in Figure 5. Comparing the Phase I models for the easiest (*Photo*) and hardest (*Sketch*) unseen domains (Figs. 5a,b), we find that `MatchDG` achieves a higher overlap between train and test domains for *Photo* than *Sketch*, highlighting the difficulty of generalizing to the *Sketch* domain, even as classes are well-separated in the training domains for both models (Figs. 5c,d).

Table 17. Accuracy on PACS with ResNet 18 (default, top row set), Resnet 18 with test domain validation (middle row set), and ResNet 50 (bottom row set). The results for JiGen (Carlucci et al., 2019), S-MLDG (Li et al., 2020), D-SAM (D'Innocente & Caputo, 2018), MMLD (Matsuura & Harada, 2020), DDAIG (Zhou et al., 2020) SagNet (Nam et al., 2019), DDEC (Asadi et al., 2019), DANN (Ganin et al., 2016), C-DANN (Li et al., 2018d), DRO (Sagawa et al., 2019), Mixup (Xu et al., 2019; Yan et al., 2020; Wang et al., 2020), IRM (Arjovsky et al., 2019), MLDG (Li et al., 2018a), MMD (Li et al., 2018b), CORAL (Sun & Saenko, 2016), were taken from the DomainBed (Gulrajani & Lopez-Paz, 2020) paper. For G2DM (Albuquerque et al., 2020a), DGER (Zhao et al., 2020), CSD (Piratla et al., 2020), MASF (Dou et al., 2019), EpiFCR (Li et al., 2019a), MetaReg (Balaji et al., 2018), RSC (Huang et al., 2020) it was taken from their respective paper.

	P	A	C	S	Average.
ERM	95.38 (0.86)	77.68 (0.35)	78.98 (0.59)	74.75 (1.70)	81.70
JiGen	96.0	79.42	75.25	71.35	80.41
MASF	94.99 (0.09)	80.29 (0.18)	77.17 (0.08)	71.69 (0.22)	81.04
G2DM	93.75	77.78	75.54	77.58	81.16
DGER	96.65 (0.21)	80.70 (0.71)	76.40 (0.34)	71.77 (1.27)	81.38
CSD	94.1 (0.2)	78.9 (1.1)	75.8 (1.0)	76.7 (1.2)	81.4
EpiFCR	93.9	82.1	77.0	73.0	81.5
MetaReg	95.5 (0.24)	83.7 (0.19)	77.2 (0.31)	70.3 (0.28)	81.7
S-MLDG	94.80	80.50	77.80	72.80	81.50
D-SAM	94.30	79.48	77.13	75.30	81.55
MMLD	96.09	81.28	77.16	72.29	81.83
DDAIG	95.30	**84.20**	78.10	74.70	83.10
SagNet	95.47	83.58	77.66	76.30	83.25
DDEC	**96.93**	83.01	79.39	78.62	84.46
RSC	95.99	83.43	80.31	**80.85**	**85.15**
`RandMatch`	95.37 (0.25)	78.16 (1.51)	78.83 (1.18)	75.13 (1.90)	81.87
`MatchDG`	95.93 (0.21)	79.77 (0.12)	80.03 (0.03)	77.11 (0.35)	83.21
`MDGHybrid`	96.15 (0.40)	81.71 (0.75)	**80.75** (0.50)	78.79 (1.25)	84.35
G2DM (Test)	94.63	81.44	79.35	79.52	83.34
`RandMatch` (Test)	95.57 (0.17)	79.09 (1.09)	79.37 (0.89)	77.60 (0.87)	82.91
`MatchDG` (Test)	96.53 (0.05)	81.32 (0.38)	80.70 (0.54)	79.72 (1.01)	84.56
`MDGHybrid` (Test)	**96.67** (0.20)	**82.80** (0.32)	**81.61** (0.06)	**81.05** (1.01)	**85.53**
DomainBed (ResNet50)	97.8 (0.0)	88.1 (0.1)	77.9 (1.3)	79.1 (0.9)	85.7
MASF (ResNet50)	95.01 (0.10)	82.89 (0.16)	80.49 (0.21)	72.29 (0.15)	82.67
C-DANN (ResNet50)	97.0 (0.4)	84.0 (0.9)	78.5 (1.5)	71.8 (3.9)	82.8
MetaReg (ResNet50)	97.6 (0.31)	87.2 (0.13)	79.2 (0.27)	70.3 (0.18)	83.6
DRO (ResNet50)	98.0 (0.3)	86.4 (0.3)	79.9 (0.8)	72.1 (0.7)	84.1
Mixup (ResNet50)	97.7 (0.2)	86.5 (0.4)	76.6 (1.5)	76.5 (1.2)	84.3
IRM (ResNet50)	96.7 (0.3)	85.0 (1.6)	77.6 (0.9)	78.5 (2.6)	84.4
DANN (ResNet50)	97.6 (0.2)	85.9 (0.5)	79.9 (1.4)	75.2 (2.8)	84.6
MLDG (ResNet50)	97.0 (0.9)	**89.1** (0.9)	78.8 (0.7)	74.4 (2.0)	84.8
MMD (ResNet50)	97.5 (0.4)	84.5 (0.6)	79.7 (0.7)	78.1 (1.3)	85.0
DGER	98.25 (0.12)	87.51 (1.03)	79.31 (1.40)	76.30 (0.65)	85.34
CORAL (ResNet50)	97.6 (0.0)	87.7 (0.6)	79.2 (1.1)	79.4 (0.7)	86.0
RSC (ResNet50)	97.92	87.89	82.16	**83.35**	**87.83**
`RandMatch` (ResNet50)	97.89 (0.11)	82.16 (0.19)	81.68 (0.45)	80.45 (0.19)	85.54
`MatchDG` (ResNet50)	97.94 (0.27)	85.61 (0.81)	82.12 (0.69)	78.76 (1.13)	86.11
`MDGHybrid` (ResNet50)	**98.36** (0.06)	86.74 (1.01)	**82.32** (0.76)	82.66 (0.48)	87.52

Table 18. Accuracy results on the PACS dataset trained with Alexnet (default, top row set), and Alexnet with test domain validation (bottom row set). The results for DBADG (Li et al., 2017), MTSSL (Albuquerque et al., 2020b), CIDDG (Li et al., 2018d), HEX (Wang et al., 2019), FeatureCritic (Li et al., 2019b), MLDG (Li et al., 2018a), REx (Krueger et al., 2020), CAADG (Rahman et al., 2020), Epi-FCR (Li et al., 2019a), MASF (Dou et al., 2019) were taken from the DomainBed (Gulrajani & Lopez-Paz, 2020) paper. The results for DANN (Ganin et al., 2016), IRM (Arjovsky et al., 2019), G2DM (Albuquerque et al., 2020a) were taken from the G2DM paper. The results for D-MTAE (Ghifary et al., 2015), MetaReg (Balaji et al., 2018), JiGen (Carlucci et al., 2019), DGER (Zhao et al., 2020) and RSC (Huang et al., 2020) were taken from the respective paper.

Method/Test Domain	Photo	Art Painting	Cartoon	Sketch	Average
ERM	85.29 (0.22)	64.23 (0.18)	66.61 (0.88)	59.25 (0.83)	68.85
D-MTAE	**91.12**	60.27	58.65	47.68	64.45
DANN	88.10	63.20	67.50	57.00	69.00
DBADG	89.50	62.86	66.97	57.51	69.21
MTSSL	84.31	61.67	67.41	63.91	69.32
CIDDG	78.65	62.70	69.73	64.45	69.40
HEX	87.90	66.80	69.70	56.30	70.20
FeatureCritic	90.10	64.40	68.60	58.40	70.40
MLDG	88.00	66.23	66.88	58.96	70.71
REx	89.74	67.04	67.97	59.81	71.14
CAADG	89.16	65.52	69.90	63.37	71.98
Epi-FCR	86.1	64.7	72.3	65.0	72.0
IRM	89.97	64.84	71.16	63.63	72.39
MetaReg	91.07 (0.41)	69.82 (0.76)	70.35 (0.63)	59.26 (0.31)	72.62
JiGen	89.00	67.63	71.71	65.18	73.38
G2DM	88.12	66.60	73.36	66.19	73.55
MASF	90.68	70.35	72.46	67.33	75.21
DGER	89.92 (0.42)	71.34 (0.87)	70.29 (0.77)	**71.15 (1.01)**	75.67
RSC	90.88	**71.62**	**75.11**	66.62	**76.05**
`RandMatch`	85.42 (0.52)	65.54 (1.14)	68.41 (1.62)	59.46 (1.35)	69.71
`MatchDG`	85.41 (0.41)	66.21 (0.64)	68.47 (1.10)	59.56 (1.24)	69.91
`MDGHybrid`	85.67 (0.67)	66.89 (1.23)	68.89 (1.08)	60.39 (2.13)	70.46
`RandMatch` (Test)	86.04 (0.47)	67.35 (0.32)	69.71 (0.56)	64.66 (1.08)	71.94
`MatchDG`(Test)	86.52 (0.43)	67.99 (0.56)	69.92 (0.09)	65.64 (1.48)	72.52
`MDGHybrid` (Test)	87.03 (0.29)	67.97 (0.79)	71.06 (0.43)	67.19 (0.44)	73.31